Article

Cell Reports

Neuronal Soma-Derived Degradative Lysosomes Are Continuously Delivered to Distal Axons to Maintain Local Degradation Capacity

Graphical Abstract

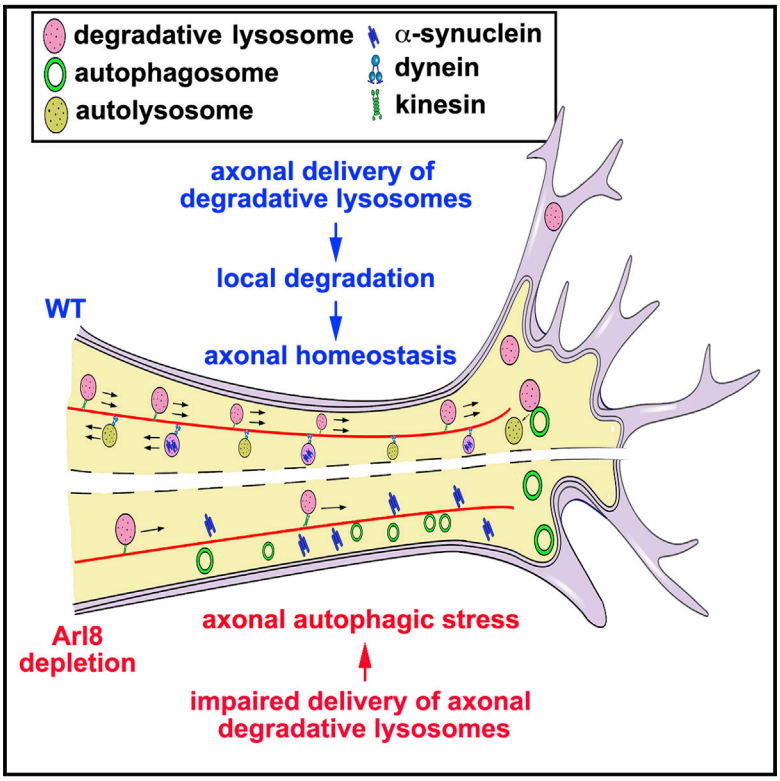

Authors

Tamar Farfel-Becker, Joseph C. Roney, Xiu-Tang Cheng, Sunan Li, Sean R. Cuddy, Zu-Hang Sheng

Correspondence

shengz@ninds.nih.gov

In Brief

The unique morphology of neurons presents a challenge to maintain cellular homeostasis through autophagic-lysosomal degradation. Farfel-Becker et al. reveal axon-targeted delivery and maintenance of degradative lysosomes by using lysosomal-activity-based probes in microfluidic devices and axons as an active compartment for local degradation. Impairing lysosome axonal delivery induces distal autophagic stress.

Highlights

- Degradative lysosomes are positioned along axons and abundant in axon tips
- Soma-labeled degradative lysosomes rapidly influx into distal axons
- Degradative lysosomes target to axonal autophagosomes and α-synuclein cargos
- Impaired delivery of degradative lysosomes induces autophagic stress in axons

Farfel-Becker et al., 2019, Cell Reports *28*, 51–64
July 2, 2019
https://doi.org/10.1016/j.celrep.2019.06.013

Cell Reports
Article

Neuronal Soma-Derived Degradative Lysosomes Are Continuously Delivered to Distal Axons to Maintain Local Degradation Capacity

Tamar Farfel-Becker,[1] Joseph C. Roney,[1] Xiu-Tang Cheng,[1] Sunan Li,[1] Sean R. Cuddy,[1] and Zu-Hang Sheng[1,2,*]
[1]Synaptic Function Section, The Porter Neuroscience Research Center, National Institute of Neurological Disorders and Stroke, National Institutes of Health, Room 2B-215, 35 Convent Drive, Bethesda, MD 20892-3706, USA
[2]Lead Contact
*Correspondence: shengz@ninds.nih.gov
https://doi.org/10.1016/j.celrep.2019.06.013

SUMMARY

Neurons face the challenge of maintaining cellular homeostasis through lysosomal degradation. While enzymatically active degradative lysosomes are enriched in the soma, their axonal trafficking and positioning and impact on axonal physiology remain elusive. Here, we characterized axon-targeted delivery of degradative lysosomes by applying fluorescent probes that selectively label active forms of lysosomal cathepsins D, B, L, and GCase. By time-lapse imaging of cortical neurons in microfluidic devices and standard dishes, we reveal that soma-derived degradative lysosomes rapidly influx into distal axons and target to autophagosomes and Parkinson disease-related α-synuclein cargos for local degradation. Impairing lysosome axonal delivery induces an aberrant accumulation of autophagosomes and α-synuclein cargos in distal axons. Our study demonstrates that the axon is an active compartment for local degradation and reveals fundamental aspects of axonal lysosomal delivery and maintenance. Our work establishes a foundation for investigations into axonal lysosome trafficking and functionality in neurodegenerative diseases.

INTRODUCTION

Lysosomes serve as degradation hubs for endocytic and autophagic components, thus maintaining cellular homeostasis essential for neuronal survival and function (Ferguson, 2018; Sharma et al., 2018; Jin et al., 2018a; Lie and Nixon, 2018). While endo-lysosomal trafficking delivers extracellular and plasma membrane proteins to lysosomes for degradation, intracellular misfolded proteins and dysfunctional organelles are engulfed within autophagosomes, which undergo fusion with endo-lysosomes to form degradative autolysosomes (Cheng et al., 2015; Feng et al., 2014; Tooze et al., 2014). Lysosomal degradation is then executed by a variety of active hydrolases that require acidic environment for their maturation and activity (Ishidoh and Kominami, 2002; Braulke and Bonifacino, 2009). Therefore, enzymatic activity is the key defining feature for degradative lysosomes.

Neurons are extremely polarized cells consisting of a small cell body, branched dendrites, and an extended long axon. This unique morphology presents an exceptional challenge for neurons to maintain cellular homeostasis by driving long-distance transport of degradation cargos and active lysosomes between the soma and distal axons. The currently accepted concept is that axonal lysosomes are mainly immature or lack degradative capacity and that degradation cargos, such as autophagosomes, must be retrogradely transported into the soma for effective degradation (Ferguson 2018). Previous studies established that lysosomal dysfunction and transport defects contribute to the pathogenesis of major neurodegenerative diseases, including Alzheimer disease, Parkinson disease, and amyotrophic lateral sclerosis (Nixon, 2013; Xie et al., 2015; Wong and Krainc, 2016; 2017; Menzies et al., 2017; Wang et al., 2018; Pitcairn et al., 2019; Klein and Mazzulli, 2018). Lysosome deficits are also linked to axonal dystrophy characterized by the formation of axonal swellings containing aberrantly accumulated degradation cargos (Walkley et al., 2010; Lee et al., 2011), highlighting the importance of lysosomes in maintaining axonal homeostasis. Axonal dystrophy is a pathological hallmark of several neurodegenerative diseases and neurological lysosomal storage disorders (LSDs) (Xie et al., 2015; Micsenyi et al., 2009; Zigdon et al., 2017; Beard et al., 2017; Futerman and van Meer, 2004; Platt et al., 2012; Pastores and Maegawa, 2013; Boland and Platt, 2015; Fraldi et al., 2016). With these clinical implications, there is a growing interest in understanding the delivery and maintenance of axonal degradative lysosomes.

Although degradative lysosomes are relatively enriched in the soma, "endo-lysosome-like" organelles, often labeled by lysosome-associated membrane proteins 1 and 2 (LAMP1/2), have also been found in axons (Overly et al., 1995; Arantes and Andrews, 2006; McGuinness et al., 2007; Song et al., 2008; Cai et al., 2010; Lee et al., 2011; Maday et al., 2012; Maday and Holzbaur, 2014; Ashrafi et al., 2014; Gowrishankar et al., 2015; 2017; Farías et al., 2017; Jin et al., 2018b). However, we and others recently revealed that LAMP1/2 are widely distributed among a heterogeneous population of non-degradative endolysosomal organelles in neurons (Cheng et al., 2018; Yap et al., 2018). These studies raise three urgent and fundamental questions as

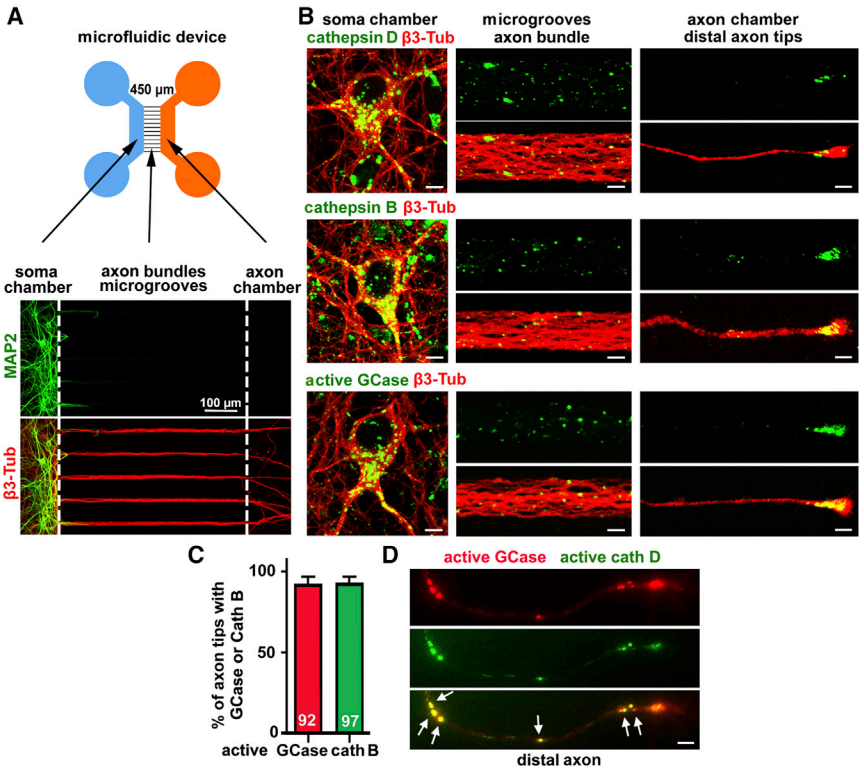

Figure 1. Lysosomal Hydrolases Are Positioned in Axons and Abundant in Distal Tips

(A) Diagram and representative images of the microfluidic device that physically separates axons from cell bodies and dendrites. Cell bodies and dendrites labeled by MAP2 (green) at DIV7 are restricted to the soma chamber, whereas axons labeled by β3-tubulin (red) grow into the axon chamber through 450-μm-long microgrooves.

(B) Images showing lysosomal hydrolases distributed in axonal terminals. Cortical neurons in microfluidic devices were co-immunostained at DIV7 with antibodies against β3-tubulin and cathepsin D (top), cathepsin B (middle), or loaded with MDW933 (500 nM for 1 h; bottom) to label active GCase. Three separated soma, microgroove, and axonal terminal compartments were imaged as indicated. Acquisition parameters were adjusted for optimal detection of lysosomes along the axons, and therefore, the signal in the soma is saturated.

(C) Quantitative analysis showing the distribution of degradative lysosomes containing cathepsin B or active GCase in the majority of axonal tips.

(D) Axonal distribution of degradative lysosomes containing active forms of both cathepsin D and GCase. Cortical neurons in microfluidic devices were loaded at DIV7 with MDW941 (5 nM) and BODIPY-FL-pepstatin A (1 μM) for 30 min in both the soma and axon chambers, followed by live imaging of distal axons in the axon chamber. Note that the majority of degradative lysosomes in distal axons are co-labeled by two active lysosomal probes (arrows) that specifically bind active GCase and cathepsin D. Data were analyzed from the total number of axon tips indicated in the bars, from 3 independent experiments (C). Error bars, SEM, scale bars, 5 μm.
See also Figures S1A and S2.

to whether (1) neurons recruit enzymatically active degradative lysosomes from the soma into distal axons to maintain local degradation capacity, (2) those degradative lysosomes have unique motility and distribution patterns in distal axons, and (3) these axon-targeted lysosomes are able to locally degrade autophagosomes and aggregate-prone mutant proteins.

Here, to address these questions, we quantitatively characterized the delivery of axonal degradative lysosomes by applying four enzymatic-activity-based fluorescent probes that selectively bind to active lysosomal hydrolases, including cathepsins D, B, and L and glucocerebrosidase (GCase) (Chen et al., 2000; Creasy et al., 2007; Kuo et al., 2018). By time-lapse imaging of cortical neurons cultured in microfluidic devices that allow physical and fluidic separation of axons from cell bodies and dendrites, we reveal that enzymatically active degradative lysosomes labeled within the soma chamber can influx into distal axons and target to autophagosomes and α-synuclein cargos for local degradation. We further show that inhibiting axonal delivery of degradative lysosomes induces aberrant accumulation of autophagosomes and mutant α-synuclein cargos in distal axons of dorsal root ganglion (DRG) neurons isolated from adult mice. Our study demonstrates that the distal axon is an active compartment for local lysosomal degradation and reveals insights into fundamental aspects of axonal lysosomal maintenance in both cortical and DRG neurons. Our findings establish a critical foundation for future investigations into axonal lysosome distribution, trafficking, and functionality in neurodegenerative diseases and LSDs associated with axonal pathology and autophagy stress (Yang et al., 2013; Tagliaferro and Burke, 2016; Haidar and Timmerman, 2017).

RESULTS

Enzymatically Active Degradative Lysosomes Are Positioned in Axons and Distal Tips

Although the majority of autophagic and endocytic organelles undergo long-distance retrograde transport from distal axons toward the soma, where degradative lysosomes are highly enriched (Cai et al., 2010; Overly et al., 1995; Maday et al., 2012; Maday and Holzbaur, 2014; Lee et al., 2011; Gowrishankar et al., 2015), elimination of damaged mitochondria and local recycling of synaptic proteins through lysosomes were also reported in axonal terminals (Ashrafi et al., 2014; Jin et al., 2018b). We hypothesized that mature degradative lysosomes containing enzymatically active hydrolases are recruited to distal axons to perform local degradation. To test our hypothesis, we used a set of activity-based fluorescent probes (Figure S1) in cortical neurons cultured in microfluidic devices that physically separate axons (labeled with β3-tubulin) from cell bodies and dendrites (labeled with MAP2) by an array of narrow 450-μm-long microgrooves (Figure 1A). This separation allows clear visualization of lysosomes distributed in distal axons. We first labeled

lysosomes by using antibodies against cathepsins, the main class of lysosomal proteases that plays an important role in the degradation of aggregate-prone proteins associated with neurodegenerative diseases (Stoka et al., 2016). By co-immunostaining cathepsin D or cathepsin B with the neuronal cytoskeleton marker β3-tubulin at day *in vitro* 7 or 8 (DIV7-8), we found that cathepsin-positive lysosomes were distributed along axon bundles and enriched in distal tips (Figure 1B). We next examined the axonal distribution of a hydrolase of a different class, the acid β-glucosidase GCase, a sphingolipid-degrading lysosomal enzyme (Grabowski et al., 1990). Active GCase can be detected by the activity-based fluorescent probes MDW933 (green) and MDW941 (red) (Witte et al., 2010; Herrera Moro Chao et al., 2015), which bind the active site of GCase in acidic lysosomes (Figure S1A), and is, therefore, a reliable marker for degradative lysosomes. We loaded neurons at DIV7-8 with MDW933 (500 nM for 1 h) to label active GCase, followed by fixation and immunostaining for β3-tubulin. Similar to the distribution pattern of cathepsins D and B, GCase puncta were detected along axon bundles and accumulated in distal tips (Figure 1B). Remarkably, the majority of axonal tips contained active GCase (92.44% ± 4.28%) or cathepsin B (93.18% ± 3.53%) (Figure 1C). To examine the co-presence of active hydrolases of two different classes within the same lysosomal organelles, we co-loaded neurons at DIV7-8 with MDW941 (5 nM for 30 min) to label active GCase and BODIPY-FL-pepstatin A (1 μM for 30 min) to label active cathepsin D (Chen et al., 2000; Figure S1B). Live-imaging revealed that the majority of lysosomes along distal axons contained active forms of both GCase and cathepsin D (Figure 1D). Thus, although enzymatically active degradative lysosomes are enriched in the soma of neurons in either standard culture dishes (Figure S2) or microfluidic devices (Figure 1B), they are also positioned along axons and abundant in distal tips.

We next verified the specificity of these activity-based probes in neurons. First, we tested the specificity of MDW941 for detecting active GCase by treating cortical neurons at DIV14 with CBE (conduritol B epoxide; 100 μM, 24 h), a selective GCase inhibitor (Zigdon et al., 2017), followed by co-loading MDW941 (100 nM, 30 min) and BODIPY-FL-pepstatin A (1 μM, 30 min) to detect active forms of GCase and cathepsin D. Blocking GCase activity abolished MDW941 labeling ($p < 0.001$) but had no effect on the labeling of cathepsin D (Figures 2A and 2B). Second, we tested the specificity of BODIPY-FL-pepstatin A for detecting active cathepsin D by treating cortical neurons at DIV14 for 24 h with pepstatin A, an inhibitor of aspartic proteases, including cathepsin D. Neurons were subsequently co-loaded with BODIPY-FL-pepstatin A (1 μM, 30 min) and MDW941 (100 nM, 30 min). Blocking cathepsin D activity abolished the labeling by BODIPY-FL-pepstatin A ($p < 0.001$) but had no effect on the labeling of active GCase (Figures 2C and 2D). In addition, we tested the specificity of the fluorogenic substrate Magic Red cathepsin B for detecting cathepsin B activity by treating neurons with E64d (10 μM, 24 h), an inhibitor of cysteine proteases, including cathepsin B. Neurons were subsequently co-loaded with Magic Red cathepsin B (1:4000) and BODIPY-FL-pepstatin A (1 μM) for 30 min. Consistently, blocking cathepsin B activity selectively abolished the labeling by Magic Red ($p < 0.001$) but had no effect on the labeling of active cathepsin D by BODIPY-FL-pepstatin A (Figures 2E and 2F). Altogether, by selectively inhibiting the activity of GCase, cathepsin D or B, we demonstrated the specific labeling of active forms of these lysosomal hydrolases by their activity-based probes.

Degradative Lysosomes Are Rapidly Delivered from the Soma to Distal Axons

The axonal positioning of degradative lysosomes suggests their delivery from the soma where mature lysosomes are highly enriched. To test this possibility, we spatially loaded MDW941 (5 nM for 1 h) in the soma-dendritic chamber, followed by time-lapse imaging of axon bundles in the microgrooves. Robust antergrade flux of soma-labeled enzymatically active degradative lysosomes toward distal axons was detected (Figure 3A; Video S1), with a mean velocity of 1.91 ± 0.04 μm/sec (Figure 3B). Next, we tested if these soma-labeled degradative lysosomes are able to transport into distal tips. The soma chamber of DIV7-8 cortical neurons was briefly loaded with MDW933 (500 nM for 15 min) and then washed. Neurons were fixed at 0, 30, 60, 90, 120, or 180 min post-wash and then immunostained for β3-tubulin. Active GCase signal in distal tips was hardly detected when neurons were fixed after 15 min of somatic loading of MDW933 (Figures 3C and 3D). As post-wash time increased to 180 min, GCase signal accumulated in distal axon tips. To exclude MDW933 diffusion in the microfluidic device, we disrupted microtubules in the soma chamber with 10 μg/ml nocodazole for 3 h before imaging MDW933 in the axonal terminals. This treatment was reported to inhibit microtubule-based lysosomal transport without affecting normal neuronal morphology (Goo et al., 2017). Disrupting somatic microtubules abolished the delivery of MDW933 to distal axonal tips, thus confirming transport, rather than diffusion, of MDW933 from the soma to axonal terminals (Figure S3).

We characterized the motility of degradative lysosomes in distal axons. After applying the active cathepsin D probe BODIPY-FL-pepstatin A (1 μM for 30 min) on both the soma and axon chambers, distal axons were time-lapse imaged at high acquisition frequency (1-s intervals) for a total of 3 min. Analysis of 53 axons revealed that the majority (68.86% ± 3.0%) of degradative lysosomes were motile, showing net displacement greater than 10 μm. A similar portion of degradative lysosomes moved in the anterograde (35.66% ± 2.25%) or retrograde (34.49% ± 2.56%) directions, reflecting a steady-state maintenance of the degradative lysosomal pool in distal axons (Figures 3E and 3F; Videos S2 and S3).

The Motility of Degradative Lysosomes in Synaptically Connected Axons of Mature Neurons

We cultured cortical neurons in standard culture dishes for 2 weeks to characterize the axonal delivery and motility of degradative lysosomes in synaptically connected axons of mature neurons. First, degradative lysosomes were revealed by loading MDW941, and presynaptic terminals were identified along axons by immunostaining for synaptophysin at DIV14 (Figure 4A). Second, in the same mature neuronal culture, the anterograde delivery of degradative lysosomes exiting the soma to a proximal axon was revealed by live imaging of proximal axonal regions

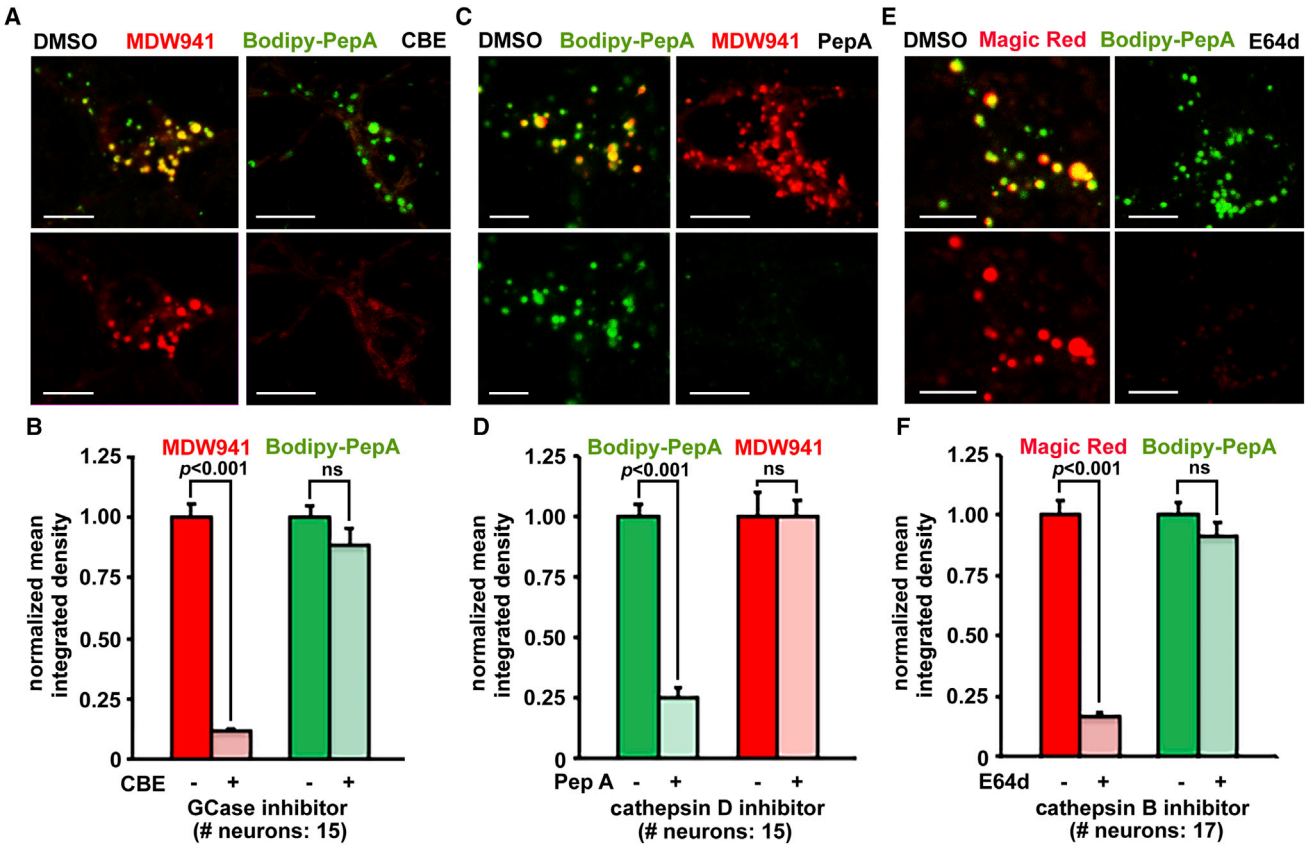

Figure 2. Specific Labeling of Active Hydrolases in Neurons

(A and B). Representative images (A) and quantitative analysis (B) showing the specificity of MDW941 for detecting active GCase. Cortical neurons at DIV14 were treated with DMSO or CBE (100 μM), a selective GCase inhibitor, for 24 h, followed by co-loading MDW941 (100 nM) and BODIPY-FL-pepstatin A (1 μM) for 30 min to label active GCase and cathepsin D, respectively. Note that inhibiting GCase activity with CBE abolished MDW941 labeling ($p < 0.001$), but had no effect on BODIPY-FL-pepstatin A labeling. See also Figure S1.

(C and D). Representative images (C) and quantitative analysis (D) showing the specificity of BODIPY-FL-pepstatin A for detecting active cathepsin D. Cortical neurons at DIV14 were treated for 24 h with DMSO or pepstatin A (10 μM), an inhibitor of aspartic proteases, including cathepsin D, followed by co-loading BODIPY-FL-pepstatin A (1 μM) and MDW941 (100 nM) for 30 min to label active forms of cathepsin D and GCase. Note that blocking cathepsin D activity abolished the labeling of BODIPY-FL-pepstatin A ($p < 0.001$) but had no effect on the labeling of MDW941.

(E and F). Representative images (E) and quantitative analysis (F) showing the specificity of Magic Red cathepsin B for detecting cleaved cathepsin B substrate. Cortical neurons at DIV14 were treated for 24 h with DMSO or E64d (10 μM), an inhibitor of cysteine proteases, including cathepsin B, followed by co-loading Magic Red cathepsin B (1:4,000) and BODIPY-FL-pepstatin A (1 μM) for 30 min. Note that blocking cathepsin B activity selectively abolished the labeling of Magic Red ($p < 0.001$) but had no effect on the labeling of BODIPY-FL-pepstatin A.

Integrated density was measured at the soma region, and data are presented as mean integrated density normalized to control from a total of 15 neurons (B and D) or 17 neurons (F); the Mann-Whitney test was used to assess significance. Error bars, SEM, Scale bars, 10 μm. n.s., $p > 0.05$.

(Figure 4B; Video S4). Third, we performed dual-channel live-imaging of distal axons to characterize the motility of MDW941-labeled lysosomes relative to presynaptic terminals labeled by synapsin. Although presynaptic terminals were largely stationary along distal axons, degradative lysosomes were highly dynamic with similar anterograde (29.39% ± 2.40%) or retrograde (34.63% ± 2.04%) motility (Figures 4C and 4D).

We next examined the relative motility of LAMP1-labeled organelles versus degradative lysosomes containing both LAMP1 and active cathepsin D in synaptically connected cortical neurons (DIV14). Of a total of 838 LAMP1-labeled organelles, 366 (44%) were degradative lysosomes co-labeled by BODIPY-FL-pepstatin A. Notably, 53.51% ± 5.53% of anterograde and 51.97% ± 5.76% of retrograde motile LAMP1-labeled organelles were degradative lysosomes. This proportion decreased to 33.26% ± 5.07% in the stationary population (Figures 4E and 4F). Interestingly, degradative lysosomes were more motile than the total population of LAMP1-labeled organelles, suggesting that degradative lysosomes undergo dynamic search for degradation cargos.

Degradative Lysosomes Target to Autophagosomes and α-Synuclein Cargos in Axons

We next examined whether degradative lysosomes locally cleave their substrates in distal axons by spatially loading Magic Red cathepsin B or L fluorogenic substrates (1:4,000 for 30 min) in the axon chamber (Figure 5A). These substrates become fluorescent upon proteolytic cleavage by cathepsin B or L,

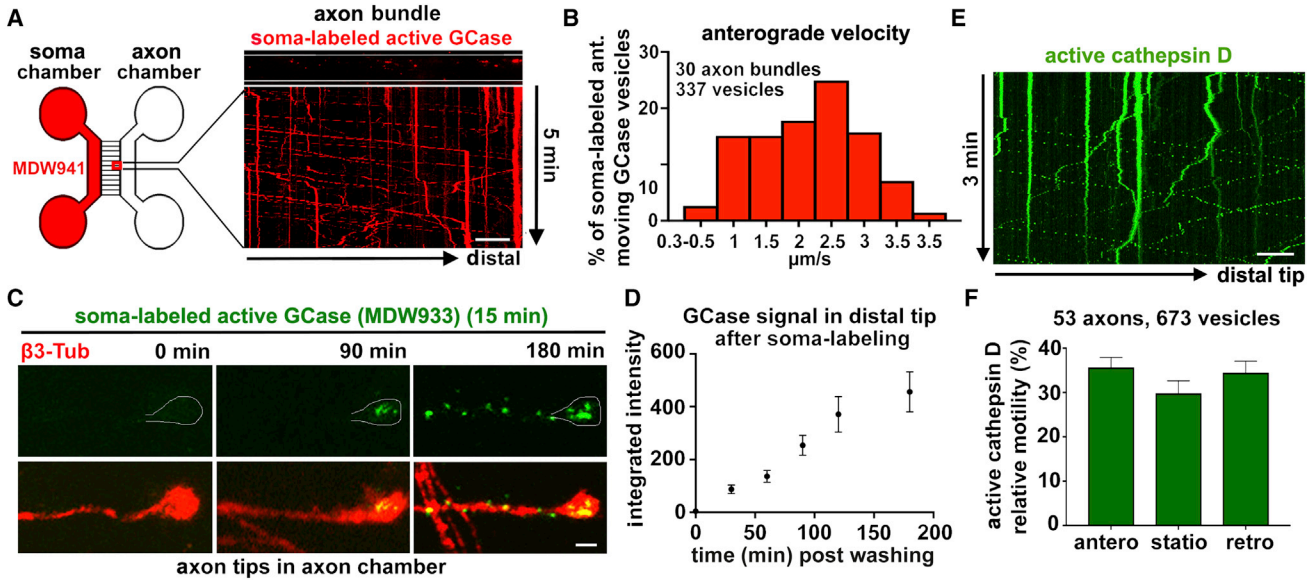

Figure 3. Degradative Lysosomes Are Rapidly Delivered from the Soma into Axons and Accumulate in Distal Tips

(A) Diagram (left), a representative single-frame live image (top right), and a corresponding kymograph (bottom right) showing the anterograde flux of degradative lysosomes from the soma chamber through long axon bundles toward distal tips. Cortical neurons were cultured in the microfluidic device and somato-dendritic lysosomes were labeled with the active GCase probe MDW941 (5 nM, 1 h) at DIV7-8, followed by 5-min time-lapse imaging with 1.3-s intervals to capture lysosome flux through axon bundles along the microgrooves (red box). The first frame and kymograph depicting the 5-min live imaging period are shown, where anterograde moving lysosomes are represented by slanted lines with a negative slope, retrograde moving ones by slanted lines with a positive slope, and stationary organelles by vertical lines.

(B) A histogram of anterograde velocities of soma-labeled degradative lysosomes in distal axons. Data were collected from a total of 337 degradative lysosomes from 30 axon bundles in 3 independent experiments. The mean anterograde velocity (1.9 ± 0.04 μm/s) was measured from active GCase-labeled motile lysosomes with net displacement ≥ 10 μM.

(C and D) Representative images (C) and quantitative analysis (D) showing the time course of degradative lysosome accumulation in distal axon tips following their labeling in the soma chamber. The soma chamber of neurons at DIV7-8 was briefly labeled by the active GCase probe MDW933 (500 nM for 15 min). Neurons were then washed and fixed after 0, 30, 60, 90, 120, or 180 minutes and immunostained for β3-tubulin. Note that active GCase signal in axon tips progressively increased following extended durations after wash, indicating the delivery of degradative lysosomes from the soma to axon tips. Data were quantified from 60 axon tips per time point and expressed as mean ± SEM.

(E and F) Representative kymograph (E) and quantitative analysis (F) showing the relative motility of degradative lysosomes in distal axons. BODIPY-FL-pepstatin A (1 μM) was applied for 30 min in both soma and axon chambers at DIV7 to label active cathepsin D. Kymographs were generated from distal axon segments over a 3-min time-lapse imaging (181.82 ms for each frame with 1-s intervals). Note that a similar portion of degradative lysosomes move in the anterograde (antero) or retrograde (retro) direction, or remain in stationary (statio) status.

Data were quantified from a total of 673 lysosomes in 53 axons from four experiments and expressed as mean ± SEM. Scale bars, 10 μm (A and E), 5 μm (C). See also Figure S3 and Videos S1, S2, and S3.

respectively, within acidic lysosomes (Creasy et al., 2007; Figures S1C and S1D). Live imaging revealed the presence of vesicular structures containing cleaved cathepsin B or L substrates along distal axons (Figures 5A and 5C). To test whether cathepsin B- or L-mediated cleavage is dependent on acidic lysosomes, we monitored substrate degradation after blocking lysosomal acidification by using bafilomycin A (50 nM, 60 min), a vacuolar H^+-pump (V-ATPase) inhibitor. Remarkably, bafilomycin A treatment largely suppressed cathepsin B- or L-mediated degradation along distal axons (Figures 5A–5D; Videos S5, S6, S7, and S8), indicating that lysosomal acidification is required for maintaining degradation capacity along distal axons.

We then determined whether these degradative lysosomes contain both locally cleaved substrates and active lysosomal enzymes. We applied BODIPY-FL-pepstatin A (1 μM, 30 min) on both soma and axon chambers to label active cathepsin D and Magic Red cathepsin B substrate (1: 4,000, 30 min) only on the axon chamber to label locally cleaved substrate of cathepsin B in distal axons (Figure 5E). Alternatively, we applied MDW933 (500 nM, 30 min) on both soma and axon chambers to label active GCase and Magic Red cathepsin L substrate (1: 4,000, 30 min) on the axon chamber to visualize cathepsin L-mediated local degradation in distal axons (Figure 5E). Live imaging of distal axons following double-labeling procedures consistently revealed co-localization of the cleaved substrates with active lysosomal enzymes, indicating that enzymatically active lysosomes locally cleave cargos in distal axons.

We next asked whether degradative lysosomes in distal axons can target to autophagosomes to form degradative autolysosomes, a critical step essential for autophagic clearance by lysosomes. Autophagosomes are constantly formed in the distal axonal tip and rapidly fuse with endo-lysosomes (Maday et al., 2012; Lee et al., 2011; Cheng et al., 2015; Farías et al., 2017). However, the degradation capacity of these hybrid organelles is largely unknown. To visualize autophagic vacuoles (AVs), we infected cortical neurons at DIV0 in microfluidic devices with a

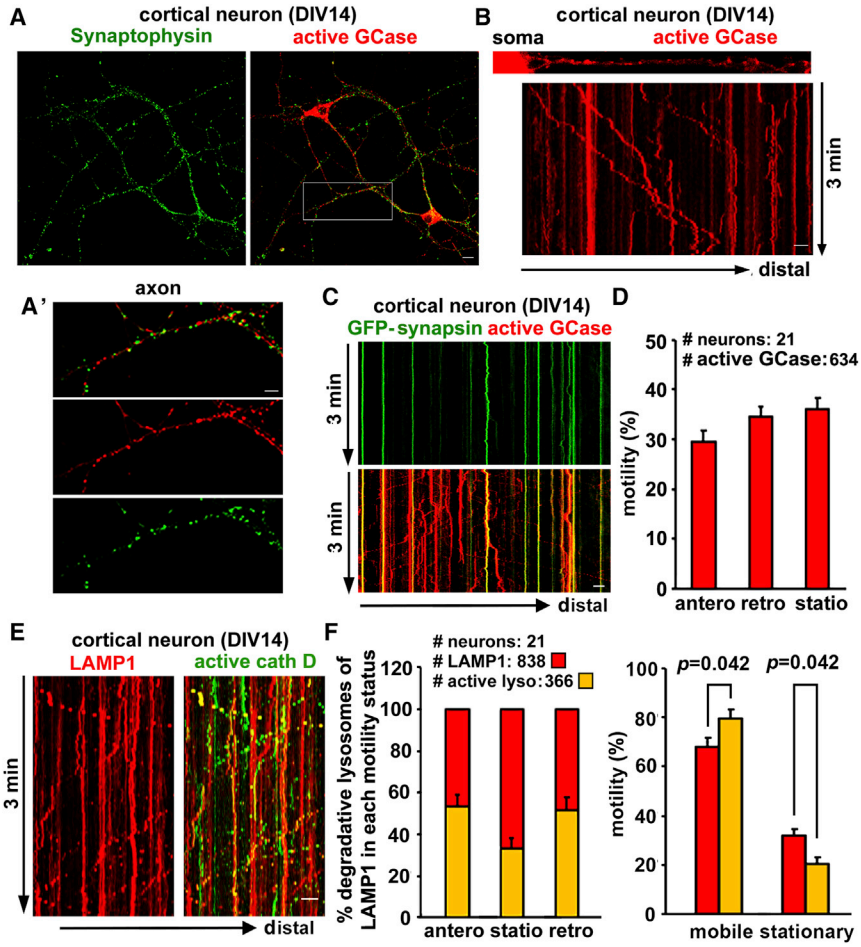

Figure 4. The Motility of Degradative and Nondegradative Lysosomes in Synaptically Connected Axons of Mature Neurons

(A) Distribution of synapses and degradative lysosomes in mature cortical neurons at DIV14. Cortical neurons at DIV14 were loaded with MDW941 to label active GCase, followed by immunostaining of synaptophysin. (A') A magnified image shows the distribution of presynapses and degradative lysosomes along an axon.

(B) Representative image of the soma and proximal axon region (upper) and corresponding kymograph (lower) showing delivery of degradative lysosomes exiting the soma into the proximal axon. Cortical neurons at DIV14 were labeled with the active GCase probe MDW941 (100 nM for 30 min), followed by 3-min time-lapse imaging. Slanted lines with a negative slope represent anterograde movement toward distal tips. See also Video S4.

(C and D) Dual-channel kymographs (C) and quantitative analysis (D) showing the motility of degradative lysosomes and presynapses in distal axons. Cortical neurons were transfected with GFP-synapsin at DIV10 and labeled with MDW941 (100 nM for 30 min) at DIV14 prior to 3-min time-lapse imaging. Green vertical lines indicate stationary presynaptic terminals and slanted red lines represent motile degradative lysosomes.

(E and F) Dual-channel kymographs (E) and quantitative analysis (F) showing the different motility patterns of degradative and non-degradative lysosomes along axons of mature neurons. Cortical neurons were transfected with mApple-LAMP1 at DIV10 and loaded with BODIPY-FL-pepstatin A at DIV14 (1 μM for 30 min) prior to 3-min time-lapse imaging. Red lines represent LAMP1-organelles and yellow lines represent degradative lysosomes containing both LAMP1 and active cathepsin D. Degradative lysosomes are more motile than the total pool of LAMP1 organelles ($p = 0.04$). Note that some green signals might originate from LAMP1-untransfected neurons. Data were quantified from a total of 838 LAMP1 organelles and 366 degradative lysosomes in 21 neurons from three experiments (D and F). Error bars, SEM. Mann-Whitney test.

Scale bar: 5 μm (A', B, C, and E) and 10 μm (A).

lentivirus encoding the autophagic marker EGFP-LC3. At DIV7-8, MDW941 was applied (5 nM, 1 h) on the soma chamber to label active GCase, followed by time-lapse imaging of distal axons in the axon chamber. EGFP-LC3 was mostly diffuse in the axonal cytosol and occasionally appeared as AV-like vesicular structures in distal tips. Soma-derived degradative lysosomes were recruited to the distal tip where they co-localized with AV structures (Figure 5F). Remarkably, a distinct population of active GCase vesicles (28.8% ± 4.6%) co-localized with EGFP-LC3 puncta along distal axons (Figures 5G and 5H), reflecting degradative autolysosomes. These autolysosomes were either stationary (50.8% ± 5.8%) or moved in the retrograde direction (42.3% ± 5.4%) and rarely moved in the anterograde direction (6.9% ± 3.8%). This biased motility pattern of autolysosomes contrasts with the bi-directional transport of degradative lysosomes along distal axons (Figures 3F and 5H), suggesting that only upon their anterograde delivery to distal axons a significant portion of degradative lysosomes fuse with autophagosomes for local clearance or retrograde transport. We further confirmed local degradation within distal autolysosomes by loading Magic Red cathepsin B or L substrates (1:4,000, 30 min) into the axon chamber of DIV7-8 cortical neurons expressing EGFP-LC3. Cathepsin D- and L-mediated degradation was readily detected within autolysosomes in distal axons (Figure 5I). Because axonal autolysosomes contained both active lysosomal hydrolases and degraded substrates, autophagic cargos can be degraded locally within distal autolysosomes.

We next tested if soma-labeled degradative lysosomes participate in axonal clearance of the aggregate-prone, disease-related α-synuclein, which is mainly degraded in lysosomes by cathepsin proteases (Sevlever et al., 2008; McGlinchey and Lee, 2015; Perrett et al., 2015). α-synuclein is aggregated in the soma and neurites in brain tissues of Parkinson disease patients (Spillantini et al., 1998), and its genomic duplications or triplications as well as missense mutations lead to familial Parkinson disease (Wong and Krainc, 2017). Moreover, α-synuclein pathology can spread between cells by trafficking of α-synuclein-fibril-containing lysosomes through tunneling nanotubes (Abounit et al., 2016; Victoria and Zurzolo, 2017). To label α-synuclein cargo, we infected cortical neurons in microfluidic devices

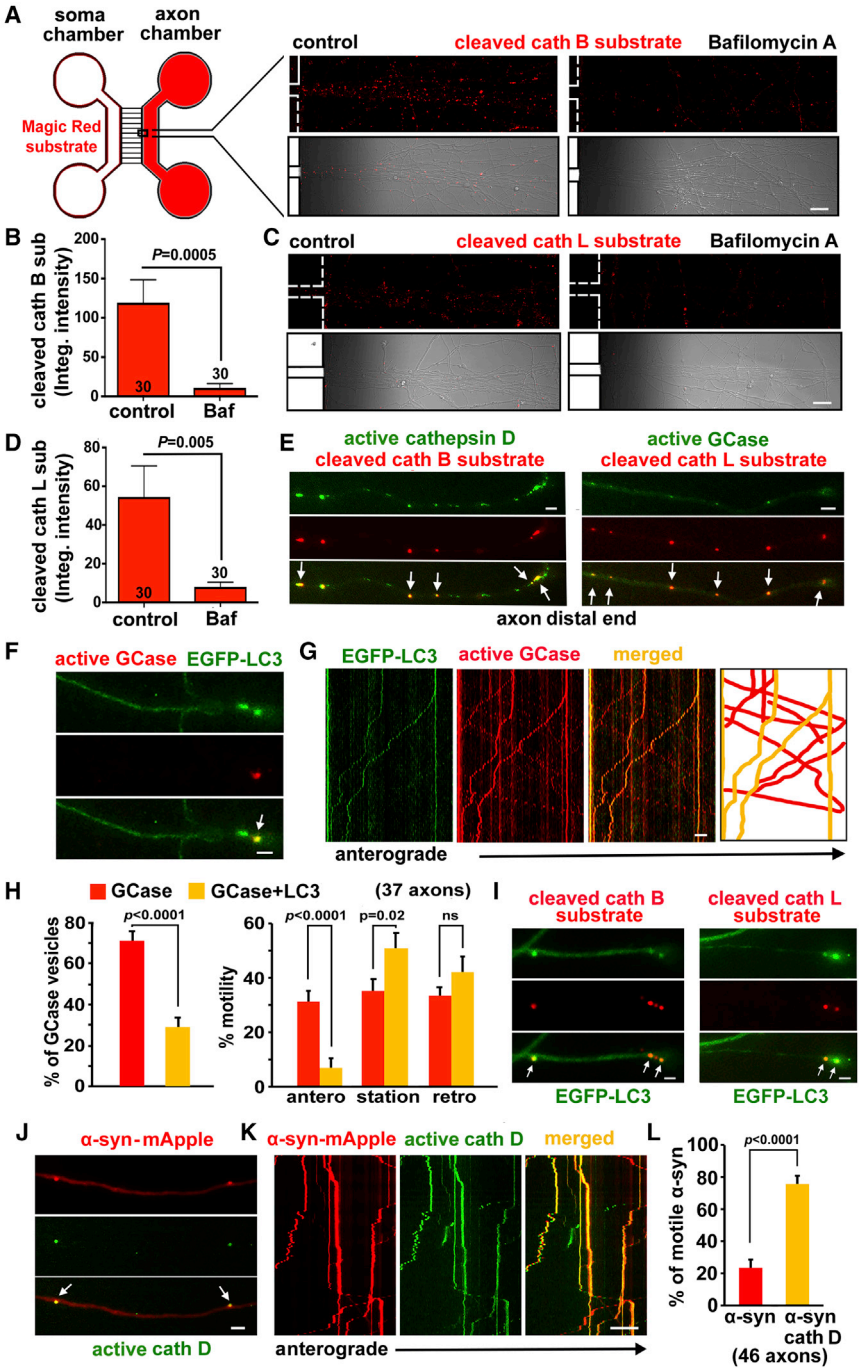

Figure 5. Distal Axons Are Degradative Compartments for Autophagosomes and α-Synuclein Cargos

(A–D) Representative images (A and C) and quantitative analyses (B and D) showing the cleavage of cathepsins B and L substrates in acidic lysosomes in distal axons. DIV7 cortical neurons cultured in microfluidic devices were loaded in both soma and axonal chambers with bafilomycin A (50 nM) for 60 min to block lysosomal acidification, followed by loading the axon chamber with Magic Red cathepsin B (A) or L (C) fluorogenic substrates (1:4,000) for 30 min. Live imaging was performed to assess acidic degradative lysosomes with cleaved Magic Red substrate. Note that bafilomycin treatment abolishes substrate cleavage. Data were quantified from the total number of axons indicated in bars. See also Figures S1C and S1D and Videos S5, S6, S7, and S8.

(E) Co-localization of active hydrolases with cleaved substrates within distal degradative lysosomes. BODIPY-FL-pepstatin A (1 μM) or MDW933 (500 nM) was applied for 30 min in both the soma and axon chambers to label degradative lysosomes. Magic Red cathepsin B or L fluorogenic substrate (1: 4,000) was applied for 30 min in the axon chamber to label cathepsin B- and cathepsin L-mediated degradation. Arrows point to degradative lysosomes containing both active cathepsins D and B (left) or active cathepsin L and GCase (right). Note that several cathepsin D organelles that do not colocalize with Magic Red may represent newly delivered lysosomes from the soma.

(F–H) Images (F), kymographs (G), and quantitative analyses (H) showing co-localization and co-migration of degradative lysosomes and autophagic vacuoles in distal axons. Cortical neurons were infected with a lentivirus encoding EGFP-LC3 and plated in microfluidic devices. At DIV7-8, MDW941 (5 nM for 1 h) was applied in the soma chamber to label active GCase. The arrow points to an autolysosome in the distal axon tip (F). Kymographs (G) represent 3 min of time-lapse imaging (2-s intervals) acquired ~100 μm away from the axon tip. Note that anterograde transport of degradative lysosomes (31.3% ± 3.8%) is largely abolished ($p < 0.0001$) when they fuse with autophagosomes to become autolysosomes (H), so that the majority of autolysosomes remain stationary (50.8% ± 5.8%) or undergo retrograde motility (42.3% ± 5.5%). Data were quantified from 37 axons in three independent experiments.

(I) Distal autolysosomes with cleavage activity. Cortical neurons were infected with a lentivirus encoding EGFP-LC3 and plated in microfluidic devices. At DIV7-8, Magic Red cathepsin B (left panel) or L (right panel) fluorogenic substrate (1: 4,000) was applied for 30 min in the axon chamber to visualize cathepsin B- and cathepsin L-mediated degradation within autolysosomes. Arrows point to autolysosomes containing cleaved substrates in the distal tip.

(J–L) Images (J), kymographs (K), and quantitative analysis (L) showing the co-localization and co-migration of degradative lysosomes and α-synuclein cargos in distal axons. Cortical neurons were infected with a lentivirus encoding α-synuclein-mApple and plated in microfluidic devices. Neurons were then loaded at DIV7-8 with BODIPY-FL-pepstatin A (1 μM) for 30 min, followed by live imaging in distal axonal segments. Arrows indicate degradative lysosomes containing α-synuclein. Kymographs were generated from 5-min time-lapse imaging with 2-s intervals at the most distal axonal segments. To exclude non-vesicular α-synuclein, co-localization was quantified from motile cargos (displacement > 2 μM) in a total of 46 axons from four independent experiments.

Error bars, SEM; unpaired t test. Scale bars, 20 μm (A and C), 10 μm (G and K), and 5 μm (E, F, I, and J). n.s., $p > 0.05$.

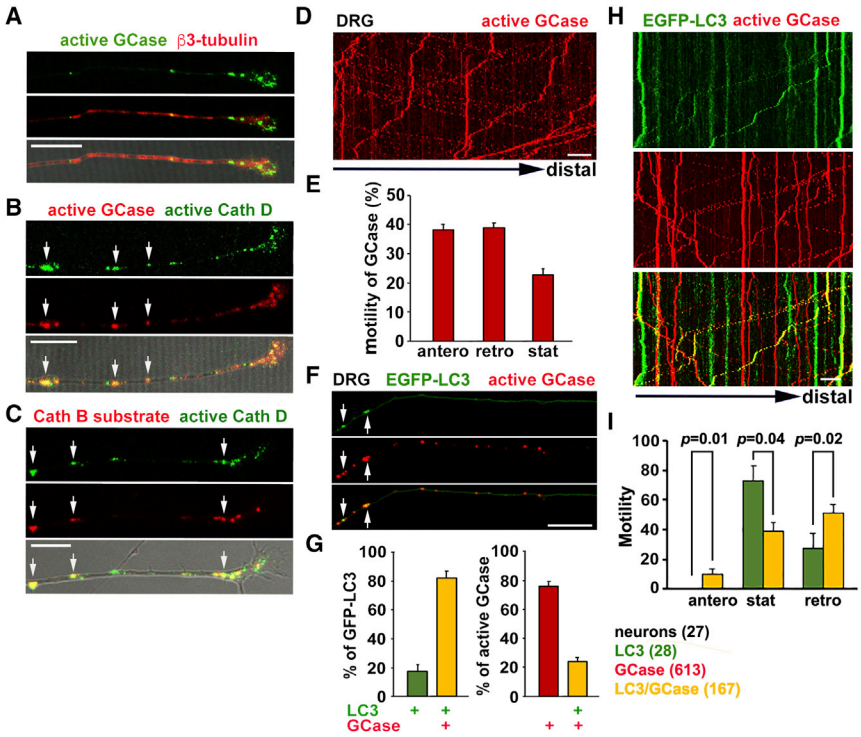

Figure 6. Characterization of Axonal Degradative Lysosomes in DRG Neurons

(A–C) Enzymatically active lysosomes are positioned in axon terminals of DRG neurons isolated from P30-40 adult mice. Neurons were loaded at DIV2-3 with MDW933 (500 nM) for 1 hour, followed by immunostaining for β3-tubulin (A), co-incubated with BODIPY-FL-pepstatin A (1 μM) and MDW941 (100 nM) (B), or co-loaded with BODIPY-FL-pepstatin A (1 μM) and the fluorogenic cathepsin B substrate Magic Red (C) (1:4000) for 30 min prior to live-imaging. Differential interference contrast (DIC) images (bottom panels) show axon growth cones. Arrows point to co-localization of active forms of cathepsin D and GCase (B) or active cathepsin D and cleaved cathepsin B substrate (C).

(D and E) Representative kymograph (D) and quantitative analysis (E) showing the bidirectional motility of degradative lysosomes in distal axons of DRG neurons. Neurons were incubated with MDW941 (100 nM) for 30 min before live-imaging at DIV2-3. Time-lapse images were collected every 1.5 s for 180 frames. See also Video S9.

(F–I) Images (F), kymographs (H), and quantitative analyses (G and I) showing colocalization of degradative lysosomes and autophagosomes as well as the relative motility of autolysosomes and autophagosomes in distal axons of DRG neurons. Neurons were nucleofected with EGFP-LC3 at DIV0 and incubated with MDW941 (100 nM) for 30 min prior to live-imaging at DIV3. Note that ~82% of autophagosomes in distal axons were co-labeled by active GCase (arrows), indicative of autolysosomes that display increased retrograde motility ($p = 0.02$) compared to autophagosomes. Data were quantified from the total number of autophagosomes (green), degradative lysosomes (red), and autolysosomes (yellow) indicated in parentheses from 27 neurons (G and I) in three independent experiments. Error bars, SEM. Mann-Whitney test. Scale bars, 10 μm.

with a lentivirus encoding α-synuclein-mApple at DIV0. Degradative lysosomes were labeled with BODIPY-FL-pepstatin A at DIV7-8, followed by dual color time-lapse imaging of distal axons. α-synuclein-mApple cargos in axons displayed bi-directional motility as previously reported (Roy et al., 2007); the majority of motile (displacement > 2 μm) α-synuclein cargos (76.08% ± 4.63) co-localized with active cathepsin D (Figures 5J–5L). Such a high degree of co-localization between α-synuclein and its degrading enzyme strongly suggests that α-synuclein can be degraded in distal axons.

Impaired Delivery of Degradative Lysosomes Induces Axonal Autophagic Stress

These findings raise a question as to whether reduced axonal delivery of degradative lysosomes impacts axonal clearance of autophagosomes and pathogenic proteins. To address this, we examined axons of cultured DRG neurons from mice at postnatal day 30–40 (P30–40). DRG neurons represent an excellent model system to study transport of axonal organelles because almost all neurites are tau-positive axons (Perlson et al., 2009) and they are amenable to isolation and culturing from adult mice. We first confirmed that degradative lysosomes were positioned along axons and enriched at distal terminals in DRG neurons; this distribution pattern was consistently observed when using the active GCase probe MDW941, the active cathepsin D probe BODIPY-FL-pepstatin A, and the fluorogenic cathepsin B substrate Magic Red (Figures 6A–6C). Degradative lysosomes in DRG axons displayed bi-directional motility (Figures 6D and 6E; Video S9) and participated in the formation of degradative autolysosomes in distal axons. Similar to our observations in cortical neurons (Figure 5H), although the majority of AVs matured into degradative autolysosomes (82.3% ± 4.4%), only a subset of degradative lysosomes (23.8% ± 3.1%) participated in AV clearance (Figures 6F and 6G). We further characterized the relative motility of LC3-labeled autophagosomes and both LC3- and active GCase-labeled autolysosomes in distal axons of DRG neurons (Figures 6H and 6I). A significantly larger portion of autophagosomes remained stationary (72.8% ± 10.5%) compared to autolysosomes (39.0% ± 4.4%, $p = 0.04$), and relatively more autolysosomes moved retrogradely (51.2% ± 6.0%, $p = 0.02$) than autophagosomes (27.2% ± 10.5%,). Those retrograde LC3-labeled AVs include amphisomes formed by fusion with late endosomes (Cheng et al., 2015). Together, these results indicate that enzymatically active lysosomes play a critical role in local degradation of axonal cargos in both central and peripheral nervous systems.

Next, we examined the outcomes of impaired lysosome delivery to axons by knocking down Arl8, a small GTPase that acts as a lysosomal kinesin adaptor. Arl8 regulates axonal transport of endo-lysosomes and presynaptic cargos (Farías et al., 2017; Klassen et al., 2010; Pu et al., 2016; Niwa et al., 2017; Rosa-Ferreira et al., 2018; Vukoja et al., 2018). In mammalian cells, Arl8

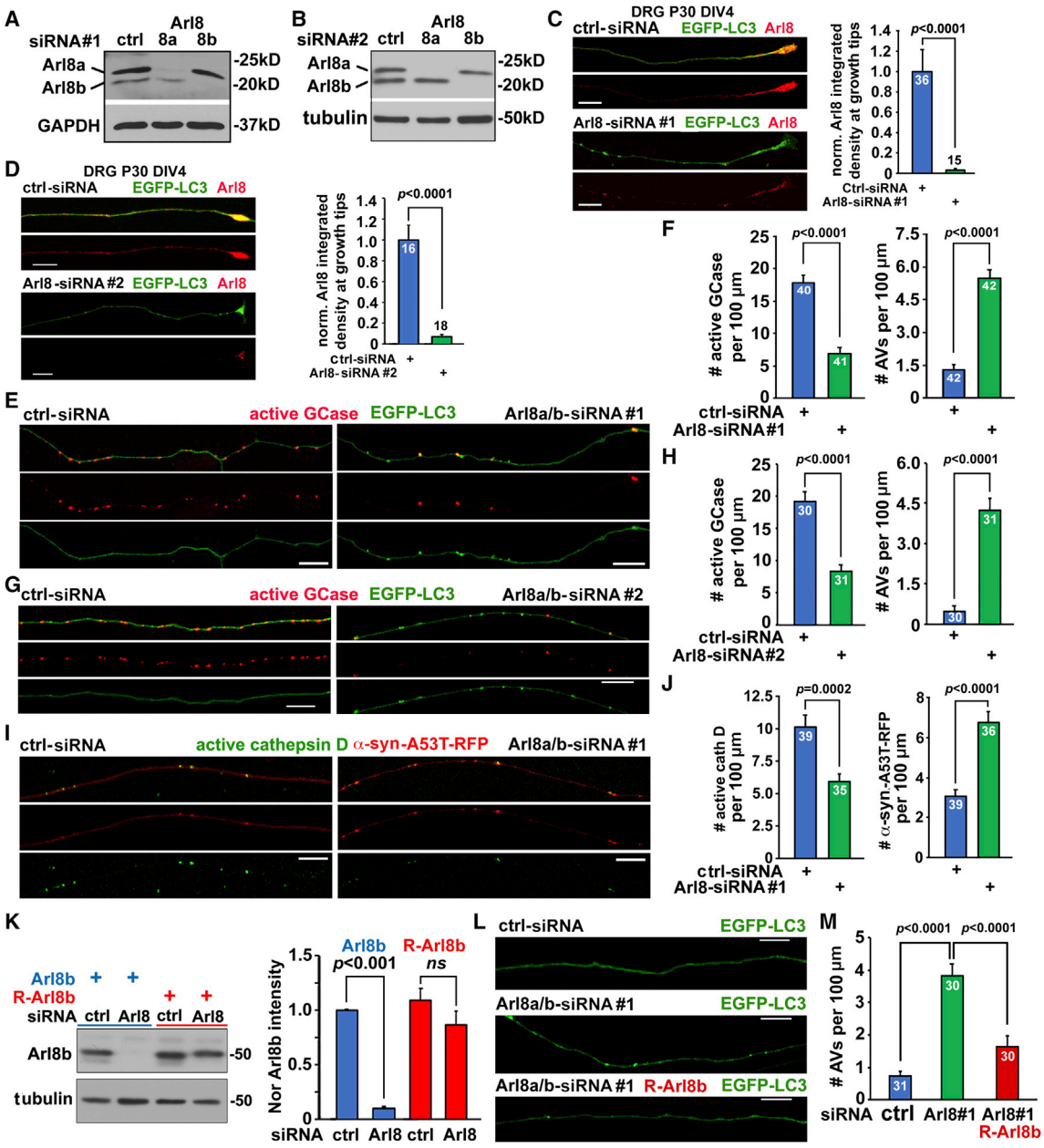

Figure 7. Impaired Axonal Delivery of Degradative Lysosomes Induces Autophagic Stress

(A and B) Immunoblots of DRG neuron lysates showing effective depletion of Arl8a/b by siRNA#1 (A) and siRNA#2 (B). DRG neurons were nucleofected with Arl8a/b-siRNA#1, -siRNA#2, or scrambled control (ctrl) at DIV0, and knock down was evaluated at DIV3 by immunoblotting equal amounts of cell lysates (6 µg) with antibodies against Arl8 and GAPDH or β3-tubulin.

(C and D) Effective Arl8 depletion in DRG neurons by siRNA#1 (C) or siRNA#2 (D). DRG neurons were co-nucleofected with EGFP-LC3 and siRNA. Knock down was assessed by immunostaining for endogenous Arl8 at DIV3-4. Integrated density of Arl8 fluorescence was measured at axonal tips by using ImageJ, and data are presented as mean integrated density normalized to ctrl-siRNA.

(E and H) Axonal autophagic stress induced by disrupting the axonal delivery of degradative lysosomes. DRG neurons were co-nucleofected at DIV0 with EGFP-LC3 together with siRNA#1 (E and F) or siRNA#2 (G and H) directed against Arl8a/b or scrambled control (ctrl). Neurons were then incubated with MDW941 (100 nM) for 30 min prior to live-imaging at DIV3-4. Note that depleting Arl8 with either siRNA#1 or siRNA#2 consistently reduced the axonal density of degradative lysosomes ($p < 0.001$), resulting in an increase in AV density in distal axons ($p < 0.001$) under non-starvation conditions.

(I and J) Axonal accumulation of mutant α-synuclein A53T caused by inhibiting the axonal delivery of degradative lysosomes. DRG neurons were co-nucleofected with α-synuclein-A53T-RFP and Arl8a/b-siRNA#1 or scrambled control (ctrl-siRNA) at DIV0. Neurons were then incubated with BODIPY-FL-pepstatin A (1 µM) for 30 min prior to live-imaging at DIV3. Note that disrupting the axonal delivery of degradative lysosomes induces axonal accumulation of mutant α-synuclein.

(K) Characterization of siRNA-resistant Arl8b mutant (R-Arl8b). R-Arl8b was generated by substituting nine nucleotides in the Arl8b-siRNA#1-targeting sequence (G459A, T462C, A463C, A465T, A468G, T471C, C474T, C477T, and T480C) without changing the amino acid sequence. HEK293T cells were co-transfected with

(legend continued on next page)

has two isoforms, namely, Arl8a and Arl8b. Both isoforms play a similar role in lysosomal positioning and motility (Bagshaw et al., 2006; Hofmann and Munro, 2006) by linking organelles to the anterograde motor kinesin-1 through its effector SKIP (Rosa-Ferreira and Munro, 2011). We reasoned that degradative lysosomes use a similar transport machinery and that knock down of Arl8 would reduce the delivery of degradative lysosomes to distal axons, leading to accumulation of lysosomal substrates and autophagic cargos. To test this, we depleted Arl8a/b expression by using two sets of small interfering RNAs (siRNAs) against different regions of Arl8a/b. Expressing Arl8a/b-siRNA#1 or Arl8a/b-siRNA#2 effectively depleted endogenous Arl8a and Arl8b in DRG neurons (Figures 7A and 7B). Knockdown efficiency was further assessed by immunostaining DRG neurons for endogenous Arl8. Consistent with a previous study (Farías et al., 2017), endogenous Arl8 is highly enriched in axonal growth cones, thus serving as a readout for the knockdown effect. Arl8 fluorescence at axonal tips was robustly suppressed ($p < 0.001$) in neurons expressing Arl8a/b-siRNA#1 or Arl8a/b-siRNA#2 compared to control siRNA (Figures 7C and 7D).

We then examined Arl8 knockdown effect on axonal delivery of degradative lysosomes and local autophagic clearance in DRG neurons. DRG neurons were co-nucleofected at DIV0 with EGFP-LC3 together with control or Arl8a/b-siRNA#1 or -siRNA#2, followed by incubation with MDW941 (100 nM, 30 min) prior to live-imaging at DIV3. In neurons expressing control siRNA, degradative lysosomes were distributed along axons, whereas EGFP-LC3 appeared mostly diffuse (Figures 7E and 7G). However, depleting Arl8 with Arl8a/b-siRNA#1 or -siRNA#2 significantly reduced the density of degradative lysosomes in axons ($p < 0.0001$) and increased AV axonal density ($p < 0.0001$), reflecting axonal autophagic stress (Figures 7F and 7H).

To exclude an off-target effect of Arl8-siRNAs, we generated an siRNA-resistant Arl8b mutant (Arl8b*) by substituting nine nucleotides in the Arl8b-siRNA#1-targeting sequence (G459A, T462C, A463C, A465T, A468G, T471C, C474T, C477T, and T480C) without changing the amino acid. Although Arl8a/b-siRNA#1 depleted endogenous Arl8 ($p < 0.001$), it failed to suppress mutant Arl8b*, indicating an siRNA-resistant Arl8b* (Figure 7K). Axonal autophagic stress induced by expressing Arl8a/b-siRNA#1 was effectively rescued by co-expressing Arl8b* ($p < 0.0001$) (Figures 7L and 7M). Altogether, by using two different sets of Arl8a/b-siRNAs combined with siRNA-resistant Arl8b*, our knockdown experiments indicate the specificity of Arl8-siRNAs.

We further examined whether impaired axonal delivery of degradative lysosomes impacts the axonal clearance of mutant α-synuclein. The A53T mutation in α-synuclein is linked to early-onset familial Parkinson disease and accelerates α-synuclein aggregation (Polymeropoulos et al., 1997; Conway et al., 1998; Narhi et al., 1999; Mazzulli et al., 2016; Wong and Krainc, 2017). Disrupting axonal delivery of degradative lysosomes in DRG neurons induced axonal accumulation of disease-relevant α-synuclein-A53T (Figures 7I and 7J). Collectively, these results demonstrate that the continuous axonal delivery of degradative lysosomes is required for the maintenance of axonal homeostasis under physiological and pathological conditions.

DISCUSSION

A long-standing question in neurobiology is whether axons have the capacity to locally degrade cargos within degradative lysosomes or if cargos must travel from remote sites to the soma where mature lysosomes are relatively enriched (Ferguson, 2018; Jin et al., 2018a). Axonal dystrophy and autophagic stress, indicators of impaired axonal transport or degradation capacity, are two hallmarks of major neurodegenerative diseases and LSDs (Xie et al., 2015; Micsenyi et al., 2009; Walkley et al., 2010; Yang et al., 2013; Tagliaferro and Burke, 2016; Zigdon et al., 2017; Beard et al., 2017; Haidar and Timmerman, 2017). Thus, it is critical to assess the distribution, transport, and degradative capacity of lysosomes in distal axons. Here, we characterized enzymatically active lysosomes by using activity-based fluorescent probes that directly label active hydrolases, instead of using nonspecific endo-lysosomal markers, such as LAMP1/2 and lysotracker (Cheng et al., 2018). Using the microfluidic culture system, our study provides direct evidence showing continuous delivery of soma-derived enzymatically active degradative lysosomes to distal axons, where they dynamically survey the axonal cytoplasm for degradation cargos to maintain axonal homeostasis. Suppressing this trafficking route induces axonal autophagic stress.

Our current study expands previous reports showing lysosomal trafficking in neurons grown in standard culture dishes where LAMP1, lysotracker, cathepsin D-GFP, or Magic Red was used to label all endo-lysosomal organelles in the soma, dendrites, and axons (Lee et al., 2011; Farías et al., 2017). These labeling approaches have a limited ability to assess lysosomal enzymatic activity and, thus, spatially determine the axonal delivery of degradative lysosomes containing active hydrolases from the soma into distal axons. Expressing cathepsin D-GFP provides limited information on the motility pattern of enzymatically active cathepsin D, given that lysosomal proteases may cleave the GFP tag within an acidic environment (Huang et al., 2014). Furthermore, it is possible that the Magic Red substrate was cleaved in the soma and then the degradation product was delivered to the distal axon within lysosomes. By focusing on axonal delivery of degradative lysosomes, our current study instead applied a unique combination of approaches (1) by using microfluidic devices to physically isolate axons from the soma and dendrites, which allows selective labeling of degradative lysosomes in the soma chamber for tracing their influx into distal

Arl8b-mCherry and ctrl-siRNA or Arl8a/b-siRNA#1, or R-Arl8b-mCherry and ctrl-siRNA or Arl8a/b-siRNA#1 as indicated, followed by immunoblotting 3 days after transfection. Equal amounts (20 μg) of cell lysates were loaded. The intensities of Arl8b-mCherry and R-Arl8b-mCherry were normalized to α-tubulin levels under the control condition (first bar). Data were from three independent experiments; unpaired Student's t test.

(L and M). Rescue of axonal autophagic stress by expressing R-Arl8b. Expressing R-Arl8b-mCherry in Arl8-depleted neurons rescues autophagic stress, as indicated by the reduced axonal density of LC3 vesicles ($p < 0.0001$) compared to un-rescued neurons. Data were collected from the total number of axons indicated within bars in three independent experiments. Error bars, SEM. One-way ANOVA. Scale bars, 10 μm. n.s., $p > 0.05$.

axons; (2) applying four different activity-dependent probes for cathepsins D, B, and L, as well as GCase, to characterize trafficking and positioning of degradative lysosomes in axons; (3) directly loading the lysosomal substrates only on the axonal chamber of the microfluidic device, which allowed us to determine the local degradation capacity in distal axons; (4) studying both young and synaptically connected mature cortical neurons as well as DRG neurons isolated from adult mice; and (5) knocking down Arl8a/b with two sets of siRNAs, combined with a rescue study using a siRNA-resistant Arl8b mutant. Our study demonstrates that degradative lysosomes are dynamically delivered to distal axons in developing and mature CNS and peripheral nervous system (PNS) neurons; disrupting the axonal delivery of degradative lysosomes induces axonal autophagic stress with build-up of autophagosomes and mutant α-synuclein cargos. We further provide evidence showing that (1) axonal cargo degradation occurs by at least two different cathepsin enzymes and (2) degradation capacity is dependent on lysosomal pH, as it is blocked by bafilomycin application.

Previous studies showed the retrograde motility of autophagosomes along with the endo-lysosomal markers LAMP1 and lysotracker (Maday et al., 2012). However, these markers do not indicate the enzymatic activity of these organelles. Our study demonstrates that autophagosomes in distal axons rapidly mature into degradative autolysosomes that contain active lysosomal enzymes and degraded cargos, thus supporting the new concept that local degradation of autophagic cargos could occur before they are transported to the soma. It is likely that axonal autophagosomes can be removed by two pathways: either through their retrograde transport toward the soma (Maday et al., 2012; Cheng et al., 2015) or through local degradation within degradative lysosomes in distal axons. As α-synuclein is a presynaptic axonal protein prone to aggregation, revealing that α-synuclein is targeted for axonal degradation within degradative lysosomes is especially important for advancing our understanding of the pathogenesis of Parkinson disease and other synucleinopathies.

Acidification of endocytic axonal organelles during their retrograde transport was previously reported using probes that were loaded to endosomes by endocytosis (Overly et al., 1995), a process likely resulting in labeling of a variety of endocytic organelles from early and late endosomes to lysosomes, and thus, the observed increase in acidification likely reflects the transition from earlier endocytic organelles to acidic lysosomes. In the current study, we instead used activity-based probes that selectively label degradative lysosomes that can be delivered to and positioned along distal axons. It is technically challenging to assess local lysosome biogenesis by blocking lysosomal bidirectional transport, which would potentially impair local maturation of the endo-lysosomal system, and thus, we cannot exclude distal lysosome biogenesis. In light of the well-established contribution of retrograde transport of endo-lysosomes to the clearance of axonal cargos, both anterograde delivery of degradative lysosomes from the soma to distal axons, as well as the retrograde trafficking of endocytic-autophagic organelles are likely to be essential to achieve effective clearance of degradative cargos in distal axons. Future investigations into the relative contribution of these two trafficking pathways by selectively disrupting kinesin versus dynein-mediated endo-lysosomal transport under physiological or pathological conditions will provide new insights into how neurons maintain axonal homeostasis in health and disease.

Our study provides a mechanistic explanation for previously reported phenotypes that genetic or pharmacological disruption of lysosomal function or axonal distribution results in increased axonal autophagic burden (Micsenyi et al., 2009; Walkley et al., 2010; Beard et al., 2017; Lee et al., 2011; Farías et al., 2017). Late endosomal and autophagic cargos undergo retrograde transport toward the soma (Hollenbeck, 1993; Cai et al., 2010; Lee et al., 2011; Cheng et al., 2015; Gowrishankar et al., 2017; Tammineni et al., 2017). It is likely that the retrograde transport of amphisomes and autolysosomes toward the soma may be required to facilitate additional fusion events with degradative lysosomes for complete degradation (Maday et al., 2012; Lee et al., 2011; Cheng et al., 2015). Our findings suggest that the lysosomal reservoir in the soma supplies "fresh" degradative lysosomes to distal axons to maintain local degradation capacity. Once reaching distal axons, these lysosomes actively cleave degradation cargos and may become stationary or switch to a bi-directional motility pattern, thus allowing efficient search for degradation cargos. The return of lysosomes back to the soma may be important for reloading lysosomes with newly synthesized lysosomal proteins from the Golgi apparatus, which is enriched in the soma (Ferguson, 2018). Lysosomes that return from distal axons to the soma may also serve as sensors of environmental or cytosolic changes and may activate signaling and transcriptional pathways to promote adaptation to such conditions (Lim and Zoncu, 2016). The fundamental insights revealed in this study provide conceptual and experimental guidelines for investigations into the regulation of transport, distribution, and degradation capacity of axonal lysosomes, thus advancing our understanding of neurodegenerative diseases characterized by early axonal dystrophy, axonal autophagic stress, and defective mutant protein clearance.

STAR★METHODS

Detailed methods are provided in the online version of this paper and include the following:

- KEY RESOURCES TABLE
- LEAD CONTACT AND MATERIALS AVAILABILITY
- EXPERIMENTAL MODEL AND SUBJECT DETAILS
  - Mice
  - Primary neuronal cultures
- METHOD DETAILS
  - Microfluidic device preparation
  - Immunofluorescence and fixed-cell imaging
  - Labeling of active lysosomal enzymes and cargo degradation
  - Characterizing the specificity of activity-based fluorescent probes
  - DNA constructs and siRNAs
  - Lentivirus production and infection
  - Live neuron imaging
  - Western blot
- QUANTIFICATION AND STATISTICAL ANALYSIS

SUPPLEMENTAL INFORMATION

Supplemental Information can be found online at https://doi.org/10.1016/j.celrep.2019.06.013.

ACKNOWLEDGMENTS

We thank members of the Sheng lab for technical assistance and constructive discussion; E. Sidransky for MDW probes and N. Morgan for design and fabrication of microfluidic device templates; and M. Ward for EGFP-LC3 lentiviral construct, J. Bonifacino for Arl8b-mCherry construct, H. Cai for α-synuclein-A53T-RFP construct, and K. Chamberlain for critical reading. This work was supported by the Intramural Research Program of NINDS, NIH ZIA NS003029 and ZIA NS002946 (Z.-H.S.), and the NINDS Competitive Postdoctoral Fellowship Award (T.F.-B.).

AUTHOR CONTRIBUTIONS

T.F.-B. developed and designed the project; T. F.-B., J.C.R., X.-T.C., S.L., and S.R.C. performed experiments and analyzed data; Z.-H.S. is the senior author who conceived and directed the project; T.F.-B., J.C.R., X.-T.C., and Z.-H.S. wrote the manuscript.

DECLARATION OF INTERESTS

The authors declare no competing financial interests.

Received: January 14, 2019
Revised: April 12, 2019
Accepted: June 4, 2019
Published: July 2, 2019

REFERENCES

Abounit, S., Bousset, L., Loria, F., Zhu, S., de Chaumont, F., Pieri, L., Olivo-Marin, J.C., Melki, R., and Zurzolo, C. (2016). Tunneling nanotubes spread fibrillar α-synuclein by intercellular trafficking of lysosomes. EMBO J. *35*, 2120–2138.

Arantes, R.M., and Andrews, N.W. (2006). A role for synaptotagmin VII-regulated exocytosis of lysosomes in neurite outgrowth from primary sympathetic neurons. J. Neurosci. *26*, 4630–4637.

Ashrafi, G., Schlehe, J.S., LaVoie, M.J., and Schwarz, T.L. (2014). Mitophagy of damaged mitochondria occurs locally in distal neuronal axons and requires PINK1 and Parkin. J. Cell Biol. *206*, 655–670.

Bagshaw, R.D., Callahan, J.W., and Mahuran, D.J. (2006). The Arf-family protein, Arl8b, is involved in the spatial distribution of lysosomes. Biochem. Biophys. Res. Commun. *344*, 1186–1191.

Beard, H., Hassiotis, S., Gai, W.P., Parkinson-Lawrence, E., Hopwood, J.J., and Hemsley, K.M. (2017). Axonal dystrophy in the brain of mice with Sanfilippo syndrome. Exp. Neurol. *295*, 243–255.

Boland, B., and Platt, F.M. (2015). Bridging the age spectrum of neurodegenerative storage diseases. Best Pract. Res. Clin. Endocrinol. Metab. *29*, 127–143.

Braulke, T., and Bonifacino, J.S. (2009). Sorting of lysosomal proteins. Biochim. Biophys. Acta *1793*, 605–614.

Cai, Q., Lu, L., Tian, J.H., Zhu, Y.B., Qiao, H., and Sheng, Z.H. (2010). Snapin-regulated late endosomal transport is critical for efficient autophagy-lysosomal function in neurons. Neuron *68*, 73–86.

Chen, C.S., Chen, W.N., Zhou, M., Arttamangkul, S., and Haugland, R.P. (2000). Probing the cathepsin D using a BODIPY FL-pepstatin A: applications in fluorescence polarization and microscopy. J. Biochem. Biophys. Methods *42*, 137–151.

Cheng, X.T., Zhou, B., Lin, M.Y., Cai, Q., and Sheng, Z.H. (2015). Axonal autophagosomes recruit dynein for retrograde transport through fusion with late endosomes. J. Cell Biol. *209*, 377–386.

Cheng, X.T., Xie, Y.X., Zhou, B., Huang, N., Farfel-Becker, T., and Sheng, Z.H. (2018). Characterization of LAMP1-labeled nondegradative lysosomal and endocytic compartments in neurons. J. Cell Biol. *217*, 3127–3139.

Conway, K.A., Harper, J.D., and Lansbury, P.T. (1998). Accelerated in vitro fibril formation by a mutant alpha-synuclein linked to early-onset Parkinson disease. Nat. Med. *4*, 1318–1320.

Creasy, B.M., Hartmann, C.B., White, F.K., and McCoy, K.L. (2007). New assay using fluorogenic substrates and immunofluorescence staining to measure cysteine cathepsin activity in live cell subpopulations. Cytometry A *71*, 114–123.

Farías, G.G., Guardia, C.M., De Pace, R., Britt, D.J., and Bonifacino, J.S. (2017). BORC/kinesin-1 ensemble drives polarized transport of lysosomes into the axon. Proc. Natl. Acad. Sci. USA *114*, E2955–E2964.

Feng, Y., He, D., Yao, Z., and Klionsky, D.J. (2014). The machinery of macroautophagy. Cell Res. *24*, 24–41.

Ferguson, S.M. (2018). Axonal transport and maturation of lysosomes. Curr. Opin. Neurobiol. *51*, 45–51.

Fraldi, A., Klein, A.D., Medina, D.L., and Settembre, C. (2016). Brain disorders due to lysosomal dysfunction. Annu. Rev. Neurosci. *39*, 277–295.

Futerman, A.H., and van Meer, G. (2004). The cell biology of lysosomal storage disorders. Nat. Rev. Mol. Cell Biol. *5*, 554–565.

Goo, M.S., Sancho, L., Slepak, N., Boassa, D., Deerinck, T.J., Ellisman, M.H., Bloodgood, B.L., and Patrick, G.N. (2017). Activity-dependent trafficking of lysosomes in dendrites and dendritic spines. J. Cell Biol. *216*, 2499–2513.

Gowrishankar, S., Yuan, P., Wu, Y., Schrag, M., Paradise, S., Grutzendler, J., De Camilli, P., and Ferguson, S.M. (2015). Massive accumulation of luminal protease-deficient axonal lysosomes at Alzheimer's disease amyloid plaques. Proc. Natl. Acad. Sci. USA *112*, E3699–E3708.

Gowrishankar, S., Wu, Y., and Ferguson, S.M. (2017). Impaired JIP3-dependent axonal lysosome transport promotes amyloid plaque pathology. J. Cell Biol. *216*, 3291–3305.

Grabowski, G.A., Gatt, S., and Horowitz, M. (1990). Acid beta-glucosidase: enzymology and molecular biology of Gaucher disease. Crit. Rev. Biochem. Mol. Biol. *25*, 385–414.

Haidar, M., and Timmerman, V. (2017). Autophagy as an emerging common pathomechanism in inherited peripheral neuropathies. Front. Mol. Neurosci. *10*, 143.

Herrera Moro Chao, D., Kallemeijn, W.W., Marques, A.R., Orre, M., Ottenhoff, R., van Roomen, C., Foppen, E., Renner, M.C., Moeton, M., van Eijk, M., et al. (2015). Visualization of active glucocerebrosidase in rodent brain with high spatial resolution following in situ labeling with fluorescent activity-based probes. PLoS One *10*, e0138107.

Hofmann, I., and Munro, S. (2006). An N-terminally acetylated Arf-like GTPase is localised to lysosomes and affects their motility. J. Cell Sci. *119*, 1494–1503.

Hollenbeck, P.J. (1993). Products of endocytosis and autophagy are retrieved from axons by regulated retrograde organelle transport. J. Cell Biol. *121*, 305–315.

Huang, L., Pike, D., Sleat, D.E., Nanda, V., and Lobel, P. (2014). Potential pitfalls and solutions for use of fluorescent fusion proteins to study the lysosome. PLoS One *9*, e88893.

Ishidoh, K., and Kominami, E. (2002). Processing and activation of lysosomal proteinases. Biol. Chem. *383*, 1827–1831.

Jin, E.J., Kiral, F.R., and Hiesinger, P.R. (2018a). The where, what, and when of membrane protein degradation in neurons. Dev. Neurobiol. *78*, 283–297.

Jin, E.J., Kiral, F.R., Ozel, M.N., Burchardt, L.S., Osterland, M., Epstein, D., Wolfenberg, H., Prohaska, S., and Hiesinger, P.R. (2018b). Live observation of two parallel membrane degradation pathways at axon terminals. Curr. Biol. *28*, 1027–1038.e4.

Kang, J.S., Tian, J.H., Pan, P.Y., Zald, P., Li, C., Deng, C., and Sheng, Z.H. (2008). Docking of axonal mitochondria by syntaphilin controls their mobility and affects short-term facilitation. Cell *132*, 137–148.

Klassen, M.P., Wu, Y.E., Maeder, C.I., Nakae, I., Cueva, J.G., Lehrman, E.K., Tada, M., Gengyo-Ando, K., Wang, G.J., Goodman, M., et al. (2010). An Arf-like small G protein, ARL-8, promotes the axonal transport of presynaptic cargoes by suppressing vesicle aggregation. Neuron *66*, 710–723.

Klein, A.D., and Mazzulli, J.R. (2018). Is Parkinson's disease a lysosomal disorder? Brain *141*, 2255–2262.

Kuo, C.L., van Meel, E., Kytidou, K., Kallemeijn, W.W., Witte, M., Overkleeft, H.S., Artola, M.E., and Aerts, J.M. (2018). Activity-based probes for glycosidases: profiling and other applications. Methods Enzymol. *598*, 217–235.

Lee, S., Sato, Y., and Nixon, R.A. (2011). Lysosomal proteolysis inhibition selectively disrupts axonal transport of degradative organelles and causes an Alzheimer's-like axonal dystrophy. J. Neurosci. *31*, 7817–7830.

Lie, P.P.Y., and Nixon, R.A. (2018). Lysosome trafficking and signaling in health and neurodegenerative diseases. Neurobiol. Dis. *122*, 94–105.

Lim, C.Y., and Zoncu, R. (2016). The lysosome as a command-and-control center for cellular metabolism. J. Cell Biol. *214*, 653–664.

Maday, S., and Holzbaur, E.L. (2014). Autophagosome biogenesis in primary neurons follows an ordered and spatially regulated pathway. Dev. Cell *30*, 71–85.

Maday, S., Wallace, K.E., and Holzbaur, E.L. (2012). Autophagosomes initiate distally and mature during transport toward the cell soma in primary neurons. J. Cell Biol. *196*, 407–417.

Mazzulli, J.R., Zunke, F., Isacson, O., Studer, L., and Krainc, D. (2016). α-Synuclein-induced lysosomal dysfunction occurs through disruptions in protein trafficking in human midbrain synucleinopathy models. Proc. Natl. Acad. Sci. USA *113*, 1931–1936.

McGlinchey, R.P., and Lee, J.C. (2015). Cysteine cathepsins are essential in lysosomal degradation of α-synuclein. Proc. Natl. Acad. Sci. USA *112*, 9322–9327.

McGuinness, L., Bardo, S.J., and Emptage, N.J. (2007). The lysosome or lysosome-related organelle may serve as a Ca2+ store in the boutons of hippocampal pyramidal cells. Neuropharmacology *52*, 126–135.

Menzies, F.M., Fleming, A., Caricasole, A., Bento, C.F., Andrews, S.P., Ashkenazi, A., Füllgrabe, J., Jackson, A., Jimenez Sanchez, M., Karabiyik, C., et al. (2017). Autophagy and neurodegeneration: pathogenic mechanisms and therapeutic opportunities. Neuron *93*, 1015–1034.

Micsenyi, M.C., Dobrenis, K., Stephney, G., Pickel, J., Vanier, M.T., Slaugenhaupt, S.A., and Walkley, S.U. (2009). Neuropathology of the Mcoln1(-/-) knockout mouse model of mucolipidosis type IV. J. Neuropathol. Exp. Neurol. *68*, 125–135.

Narhi, L., Wood, S.J., Steavenson, S., Jiang, Y., Wu, G.M., Anafi, D., Kaufman, S.A., Martin, F., Sitney, K., Denis, P., et al. (1999). Both familial Parkinson's disease mutations accelerate alpha-synuclein aggregation. J. Biol. Chem. *274*, 9843–9846.

Niwa, S., Tao, L., Lu, S.Y., Liew, G.M., Feng, W., Nachury, M.V., and Shen, K. (2017). BORC regulates the axonal transport of synaptic vesicle precursors by activating ARL-8. Curr. Biol. *27*, 2569–2578.e4.

Nixon, R.A. (2013). The role of autophagy in neurodegenerative disease. Nat. Med. *19*, 983–997.

Overly, C.C., Lee, K.D., Berthiaume, E., and Hollenbeck, P.J. (1995). Quantitative measurement of intraorganelle pH in the endosomal-lysosomal pathway in neurons by using ratiometric imaging with pyranine. Proc. Natl. Acad. Sci. USA *92*, 3156–3160.

Pastores, G.M., and Maegawa, G.H. (2013). Clinical neurogenetics: neuropathic lysosomal storage disorders. Neurol. Clin. *31*, 1051–1071.

Perlson, E., Jeong, G.B., Ross, J.L., Dixit, R., Wallace, K.E., Kalb, R.G., and Holzbaur, E.L. (2009). A switch in retrograde signaling from survival to stress in rapid-onset neurodegeneration. J. Neurosci. *29*, 9903–9917.

Perrett, R.M., Alexopoulou, Z., and Tofaris, G.K. (2015). The endosomal pathway in Parkinson's disease. Mol. Cell. Neurosci. *66*, 21–28.

Pitcairn, C., Wani, W.Y., and Mazzulli, J.R. (2019). Dysregulation of the autophagic-lysosomal pathway in Gaucher and Parkinson's disease. Neurobiol. Dis. *122*, 72–82.

Platt, F.M., Boland, B., and van der Spoel, A.C. (2012). The cell biology of disease: lysosomal storage disorders: the cellular impact of lysosomal dysfunction. J. Cell Biol. *199*, 723–734.

Polymeropoulos, M.H., Lavedan, C., Leroy, E., Ide, S.E., Dehejia, A., Dutra, A., Pike, B., Root, H., Rubenstein, J., Boyer, R., et al. (1997). Mutation in the alpha-synuclein gene identified in families with Parkinson's disease. Science *276*, 2045–2047.

Pu, J., Guardia, C.M., Keren-Kaplan, T., and Bonifacino, J.S. (2016). Mechanisms and functions of lysosome positioning. J. Cell Sci. *129*, 4329–4339.

Rosa-Ferreira, C., and Munro, S. (2011). Arl8 and SKIP act together to link lysosomes to kinesin-1. Dev. Cell *21*, 1171–1178.

Rosa-Ferreira, C., Sweeney, S.T., and Munro, S. (2018). The small G protein Arl8 contributes to lysosomal function and long-range axonal transport in *Drosophila*. Biol. Open *7*, bio035964.

Roy, S., Winton, M.J., Black, M.M., Trojanowski, J.Q., and Lee, V.M. (2007). Rapid and intermittent cotransport of slow component-b proteins. J. Neurosci. *27*, 3131–3138.

Sevlever, D., Jiang, P., and Yen, S.H. (2008). Cathepsin D is the main lysosomal enzyme involved in the degradation of alpha-synuclein and generation of its carboxy-terminally truncated species. Biochemistry *47*, 9678–9687.

Sharma, J., di Ronza, A., Lotfi, P., and Sardiello, M. (2018). Lysosomes and Brain Health. Annu. Rev. Neurosci. *41*, 255–276.

Song, J.W., Misgeld, T., Kang, H., Knecht, S., Lu, J., Cao, Y., Cotman, S.L., Bishop, D.L., and Lichtman, J.W. (2008). Lysosomal activity associated with developmental axon pruning. J. Neurosci. *28*, 8993–9001.

Spillantini, M.G., Crowther, R.A., Jakes, R., Hasegawa, M., and Goedert, M. (1998). alpha-Synuclein in filamentous inclusions of Lewy bodies from Parkinson's disease and dementia with lewy bodies. Proc. Natl. Acad. Sci. USA *95*, 6469–6473.

Stoka, V., Turk, V., and Turk, B. (2016). Lysosomal cathepsins and their regulation in aging and neurodegeneration. Ageing Res. Rev. *32*, 22–37.

Tagliaferro, P., and Burke, R.E. (2016). Retrograde axonal degeneration in Parkinson disease. J. Parkinsons Dis. *6*, 1–15.

Tammineni, P., Ye, X., Feng, T., Aikal, D., and Cai, Q. (2017). Impaired retrograde transport of axonal autophagosomes contributes to autophagic stress in Alzheimer's disease neurons. eLife *6*, e21776.

Tooze, S.A., Abada, A., and Elazar, Z. (2014). Endocytosis and autophagy: exploitation or cooperation? Cold Spring Harb. Perspect. Biol. *6*, a018358.

Victoria, G.S., and Zurzolo, C. (2017). The spread of prion-like proteins by lysosomes and tunneling nanotubes: Implications for neurodegenerative diseases. J. Cell Biol. *216*, 2633–2644.

Vukoja, A., Rey, U., Petzoldt, A.G., Ott, C., Vollweiter, D., Quentin, C., Puchkov, D., Reynolds, E., Lehmann, M., Hohensee, S., et al. (2018). Presynaptic biogenesis requires axonal transport of lysosome-related vesicles. Neuron *99*, 1216–1232.e7.

Walkley, S.U., Sikora, J., Micsenyi, M., Davidson, C., and Dobrenis, K. (2010). Lysosomal compromise and brain dysfunction: examining the role of neuroaxonal dystrophy. Biochem. Soc. Trans. *38*, 1436–1441.

Wang, C., Telpoukhovskaia, M.A., Bahr, B.A., Chen, X., and Gan, L. (2018). Endo-lysosomal dysfunction: a converging mechanism in neurodegenerative diseases. Curr. Opin. Neurobiol. *48*, 52–58.

Westbroek, W., Nguyen, M., Siebert, M., Lindstrom, T., Burnett, R.A., Aflaki, E., Jung, O., Tamargo, R., Rodriguez-Gil, J.L., Acosta, W., et al. (2016). A new glucocerebrosidase-deficient neuronal cell model provides a tool to probe pathophysiology and therapeutics for Gaucher disease. Dis. Model. Mech. *9*, 769–778.

Witte, M.D., Kallemeijn, W.W., Aten, J., Li, K.Y., Strijland, A., Donker-Koopman, W.E., van den Nieuwendijk, A.M., Bleijlevens, B., Kramer, G., Florea,

B.I., et al. (2010). Ultrasensitive in situ visualization of active glucocerebrosidase molecules. Nat. Chem. Biol. *6*, 907–913.

Wong, Y.C., and Krainc, D. (2016). Lysosomal trafficking defects link Parkinson's disease with Gaucher's disease. Mov. Disord. *31*, 1610–1618.

Wong, Y.C., and Krainc, D. (2017). α-synuclein toxicity in neurodegeneration: mechanism and therapeutic strategies. Nat. Med. *23*, 1–13.

Xie, Y., Zhou, B., Lin, M.Y., Wang, S., Foust, K.D., and Sheng, Z.H. (2015). Endolysosomal deficits augment mitochondria pathology in spinal motor neurons of asymptomatic fALS mice. Neuron *87*, 355–370.

Yang, Y., Coleman, M., Zhang, L., Zheng, X., and Yue, Z. (2013). Autophagy in axonal and dendritic degeneration. Trends Neurosci. *36*, 418–428.

Yap, C.C., Digilio, L., McMahon, L.P., Garcia, A.D.R., and Winckler, B. (2018). Degradation of dendritic cargos requires Rab7-dependent transport to somatic lysosomes. J. Cell Biol. *217*, 3141–3159.

Zigdon, H., Meshcheriakova, A., Farfel-Becker, T., Volpert, G., Sabanay, H., and Futerman, A.H. (2017). Altered lysosome distribution is an early neuropathological event in neurological forms of Gaucher disease. FEBS Lett. *591*, 774–783.

STAR★METHODS

KEY RESOURCES TABLE

REAGENT or RESOURCE	SOURCE	IDENTIFIER
Antibodies		
Mouse anti-MAP2	BD Biosciences	Cat #556320; RRID: AB_396359
Rabbit anti-β3-tubulin	Millipore	Cat# AB5622, RRID:AB_91939
Mouse anti-β3-tubulin	Sigma-Aldrich	Cat# T8578, RRID:AB_1841228
Mouse anti-α-tubulin	Abcam	Cat# ab7291,RRID:AB_2241126
Mouse anti-mCherry	Abcam	Cat# ab125096 RRID:AB_11133266
Goat anti-cathepsin B	R and D Systems	Cat# AF965, RRID:AB_2086949
Rabbit anti-Arl8	Proteintech	Cat# 13049-1-AP; RRID:AB_2059000
Rat anti-cathepsin D	R and D Systems	Cat# MAB1029, RRID:AB_2292411
Rabbit anti-synaptophysin	Santa Cruz Biotechnology	Cat# SC-9116 RRID:AB_2199007
Goat anti-mouse, Alexa 546 Conjugate Secondary Antibody	Thermo Fisher Scientific	Cat# A-11018, RRID:AB_2534085
Goat anti-mouse, Alexa 488 Conjugate Secondary Antibody	Thermo Fisher Scientific	Cat# A-11017, RRID:AB_2534084
Donkey anti-rabbit, Alexa 488 Conjugate Secondary Antibody	Thermo Fisher Scientific	Cat# A-21206, RRID:AB_2535792
Donkey anti-rabbit, Alexa 488 Conjugate Secondary Antibody	Molecular Probes	Cat# A-11055, RRID:AB_142672
Chemicals, Peptides, and Recombinant Proteins		
MDW941, MDW933	A gift from Dr. Ellen Sidransky (Westbroek et al., 2016)	N/A
BODIPY-pepstatin-FL	Thermo Fisher Scientific	Cat# P12271
Magic Red Cathepsin B	ImmunoChemistry Technologies	Cat# 937
Magic Red Cathepsin L	ImmunoChemistry Technologies	Cat# 941
Conduritol B Epoxide (CBE)	Sigma-Aldrich	Cat# C5424
E64d	Millipore	Cat# 330005
Pepstatin A	Millipore	Cat# 516481
Bafilomycin A1	Sigma-Aldrich	Cat# SML1661
Nocodazole	Sigma-Aldrich	Cat# M1404
Bouin's solution	Sigma-Aldrich	Cat# HT10132
Poly-ornithine	Sigma-Aldrich	Cat# P4957
Laminin	Roche	Cat# 11243217001
DMEM	Thermo Fisher Scientific	Cat# 11995-065
Neurobasal	Thermo Fisher Scientific	Cat# 21103-049
Neurobasal-A	Thermo Fisher Scientific	Cat# 10888-022
Fetal Bovine Serum	HyClone	Cat# SH30071.03
B27	Thermo Fisher Scientific	Cat# 17504-044
Glutamax	Thermo Fisher Scientific	Cat# 35050-61
Low Fluorescence Hibernate E media	BrainBits	Cat# HELF
Low Fluorescence Hibernate A media	BrainBits	Cat# HALF
Beta-Mercaptoethanol	Thermo Fisher Scientific	Cat# 21985-023
FluoroGel with tris buffer	Electron Microscopy System	Cat# 17985-10
Dow Corning Sylgard 184 Silicone Encapsulant Clear 0.5 kg Kit	Ellsworth Adhesives	Cat# 184 SIL ELAST KIT 0.5KG
Dispase II	Roche	Cat# 049420780010
Collagenase	Worthington	Cat# LS004176

(*Continued on next page*)

Continued		
REAGENT or RESOURCE	SOURCE	IDENTIFIER
Critical Commercial Assays		
Basic Neuron SCN Nucleofector® Kit	Lonza	Cat# VSPI-1003
Experimental Models: Cell Lines		
HEK293T	ATCC	Cat# CRL-3216, RRID: CVCL_0063
Experimental Models: Organisms/Strains		
C57BL/6J	The Jackson Laboratory	JAX: 000664
BALB/c		N/A
Oligonucleotides		
Arl8a siRNA#1 ID MSS290361	Thermo Fisher Scientific	Cat# 1320001
Arl8b siRNA#1 ID MSS289173	Thermo Fisher Scientific	Cat# 1320001
Arl8a siRNA#2 ID MSS229276	Thermo Fisher Scientific	Cat# 1320001
Arl8b siRNA#2 ID MSS289171	Thermo Fisher Scientific	Cat# 1320001
Recombinant DNA		
pLEX PGK-EGFP-LC3	This study	N/A
pLEX PGK-SNCA-mApple	This study	N/A
pMD2.G	A gift from Dr. Didier Torno	Addgene plasmid #12259
psPAX2	A gift from Dr. Didier Torno	Addgene plasmid # 12260
EGFP-LC3	(Cheng et al., 2015)	N/A
α-Synuclein-A53T-RFP	A gift from Dr. Huaibin Cai	N/A
mApple-LAMP1	Addgene	Cat# 54627
Arl8b-mCherry	A gift from Dr. Juan Bonifacino	N/A
R-Arl8b-mCherry	This study	N/A
Software and Algorithms		
ImageJ	NIH	https://imagej.nih.gov/ij, RRID: SCR_003070
Prism 7	GraphPad Software	https://www.graphpad.com/, RRID: SCR_002798

LEAD CONTACT AND MATERIALS AVAILABILITY

Further information and requests for resources and reagents (*with the exception of MDW probes*) should be directed to and will be fulfilled by the Lead Contact, Zu-Hang Sheng (shengz@ninds.nih.gov).

EXPERIMENTAL MODEL AND SUBJECT DETAILS

Mice

All animal procedures were carried out following NIH guidelines and were approved by the NINDS/NIDCD Animal Care and Use Committee.

Primary neuronal cultures

Mouse cortical neuron cultures were prepared from cortical tissues of E18-19 B6 mouse embryos (Harlan) (sex: random) or from E18-19 BALB/c mouse embryos (sex: random) using the papain method as described previously (Kang et al., 2008). In brief, after dissociation by papain (Worthington), neurons were re-suspended in plating medium (Neurobasal medium supplemented with 2% B-27, 0.5 mM GlutaMAX, 55 μM 2-Mercaptoethanol (all from ThermoFisher Scientific), Insulin (30 μg/ml, Sigma) and 10% Fetal Bovine Serum (HyClone)) and plated at a density of 300,000 cells per 12 mm Poly-D-Lysin/Laminin pre-coated circular cover glass (Corning BioCoat) in a 24-well tissue culture plate. Twenty-four hours after plating, half of the plating medium was replaced with the same amount of neuronal feeding medium (NFM) (2% B27, 0.5 mM GlutaMAX, and 55 μM 2-Mercaptoenthanol in Neurobasal medium) containing AraC (2 μM, Sigma) to inhibit glia proliferation. One-fourth of the medium was replaced with NFM after 4 days *in vitro* (DIV4). Alternatively, 200,000 neurons in 20 μl plating medium were added into the soma well of a microfluidic device and 20 μl plating medium was added into the axon well. After cells were attached to the main channel (10 min), wells were filled with plating medium (~400 μl in total), such that axon wells contained more medium than soma wells to inhibit cells from crossing from the soma to axon compartment. Half of the medium was replaced with the same volume of NFM after 24 hours and at DIV4. Microfluidic devices were attached immediately before plating to dry 35-mm glass coverslips pre-coated with poly-ornithine (Sigma; 1:4 in PBS) and laminin

(Roche; diluted 1:500 in PBS). For synaptic connected neuronal culture, cortical neurons were plated onto 12-mm coverslips coated with poly-orthinine (Sigma; 1:4 in PBS). After 24 hr, half of the plating medium was replaced with the same volume of NFM and neurons were fed every three days. Neurons were transfected with various constructs at DIV10 using the calcium phosphate method, and imaged at DIV14 with confocal microscopy.

DRG neurons were isolated from postnatal day 30-40 (P30-40) BALB/c mice that were anesthetized with 2.5% avertin and transcardially perfused with ice-cold perfusion buffer to remove blood, reduce metabolic toxicity, and improve cell survival. After bisecting the spinal canal to expose the spinal cord, DRGs were removed and transferred to Hank's buffered salt solution supplemented with HEPES and antibiotics (all from Thermo Fisher Scientific). After excess dorsal roots were trimmed off, DRGs were digested in 2.5 units/mL dispase II (Roche) and 200 units/mL collagenase (Worthington) at 37°C for 30 min followed by 35 min of gentle rotation at room temperature. After filtering debris with a 70 μm nylon strainer (Sigma), neurons were collected and nucleofected with EGFP-LC3 or α-Synuclein-A53T-RFP and various Stealth siRNA oligonucleotides and Arl8b-mCherry or siRNA-resistant Arl8b using a Nucleofector device (Lonza) according to the manufacturer's specifications. DRG neurons were then plated on coverslips coated with 20 μg/mL poly-L-ornithine and 10 μg/mL laminin and maintained in Neurobasal-A medium (Thermo Fisher Scientific) supplemented with 2.5% fetal bovine serum, 0.5 mM GlutaMAX, 2% B27 for 2-3 days at 37°C with 5% CO_2.

METHOD DETAILS

Microfluidic device preparation

A silicon wafer with a pattern made out of SU-8 by photolithography was used to cast PDMS microfluidic devices in-house. SYLGARD 184 SILICONE elastomer base was mixed with curing agent at a ratio of 10:1. PDMS was then thoroughly mixed using a THINKY mixer ARF-310 in two steps: mixing at 2000 rpm for 4 min and de-foaming at 2200 rpm for 4 min. The well-mixed PDMS was poured onto the silicon wafer and then placed in a Bel-Art vacuum desiccator for 3 hours to help remove air bubbles from the PDMS. The wafer with PDMS was placed in an 80°C oven for 1 hour to cure. Once the PDMS was cured, it was pulled out, and reservoirs were punched out. The PDMS devices were washed and sterilized before use.

Immunofluorescence and fixed-cell imaging

Microfluidic devices were carefully removed from coverslips before fixation. DIV7 neurons were briefly rinsed in warm PBS and fixed in 4% sucrose (Sigma) Bouin's solution (Sigma) for 30 min, then washed in PBS 3 times. Neurons were permeabilized with 0.1% Triton X-100 for 10 min, washed 3 times with PBS, incubated for 30 min in blocking buffer (PBS containing 2% BSA (Sigma) and 5% goat or donkey serum (Sigma)), then incubated with primary antibodies in blocking buffer overnight at 4°C. Primary antibodies were as follows: mouse anti- MAP2 (1:1000, BD Biosciences), mouse anti-β3-Tubulin (1:5,000, Sigma), rat anti-cathepsin D (1: 400, R&D systems), goat anti-cathepsin B (1:200, R&D Systems) and rabbit anti-Arl8 (1:1000, Proteintech), and rabbit anti-synaptophysin (1:400, Santa Cruz). After 3 PBS washes, secondary antibodies (Alexa 488 or 546 conjugated, 1:500, Molecular Probes) were applied for 30 min, and cells were then washed and mounted on microscope slides (Globe Scientific). Confocal images were obtained using an Olympus Fluoview FV1000 confocal microscope with a 1.45 NA 63 × objective with sequential acquisition setting or using a Zeiss 880 confocal microscope with a 40 × 1.3 NA oil immersion objective. For fluorescence quantification, images were acquired using the same below saturation settings. Low magnification images of the microfluidic culture were acquired using a Nikon Eclipse Ti microscope with a 10 × objective.

Labeling of active lysosomal enzymes and cargo degradation

Red fluorescent MDW941 (5 or 100 nM) and green fluorescent MDW933 (500 nM) were used to label active GCase (Witte et al., 2010) and were a gift from Dr. E. Sidransky (NIH/NHGRI) (Westbroek et al., 2016). BODIPY-pepstatin-FL (1 μM, Thermo Fisher Scientific) was used to label active cathepsin D. For lysosome anterograde delivery assays, 100 μL of NFM containing fluorescent probe was applied on the soma chamber, while applying 200 μL NFM without probe on the axon chamber to maintain fluidic separation between soma and axon chambers. For fixed-cell imaging, live neurons were incubated with MDW933 (500 nM) applied on both soma and axon compartments for 1 hour to label all active GCase containing lysosomes, or with MDW933 (500 nM) applied only on the soma compartment for 15 min followed by varying washing times in NFM as indicated to label active GCase containing lysosomes delivered to distal axons. MDW933 labeled neurons were fixed and immunolabeled for β3-Tubulin as described above. For live imaging, neurons were incubated in NFM containing the various probes for 30 min at 37°C, followed by 3 washes with NFM.

For labeling lysosomal cargo degradation in axons, Magic Red Cathepsin B/L fluorogenic substrates (1:4,000, ImmunoChemistry Technologies) were applied to the axonal chamber for 30 min at 37°C to monitor Cathepsin B/L-mediated degradation.

Characterizing the specificity of activity-based fluorescent probes

For verifying the specificity of MDW941 for active GCase: cortical neurons at DIV14 were treated with DMSO as a control or 100 μM of the GCase inhibitor CBE (Sigma) for 24 hours, followed by co-loading MDW941 (100 nM, 30 min) and BODIPY-FL-pepstatin A (1 μM, 30 min) to label active GCase and cathepsin D, respectively. For verifying the specificity of BODIPY-FL-pepstatin A for active cathepsin D: cortical neurons at DIV14 were treated for 24 hours with DMSO as a control or 10 μM of pepstatin A (Millipore), an inhibitor of cathepsin D, followed by co-loading BODIPY-FL-pepstatin A (1 μM, 30 min) and MDW941 (100 nM, 30 min) to label active

forms of cathepsin D and GCase, respectively. For verifying the specificity of Magic Red cathepsin B for active cathepsin B: cortical neurons at DIV14 were treated for 24 hours with DMSO as a control or 10 μM E64d (Millipore), an inhibitor of cathepsin B, followed by co-loading Magic Red cathepsin B (1:4000) and BODIPY-FL-pepstatin A (1 μM) for 30 min.

DNA constructs and siRNAs

EGFP-LC3 was generated in Dr. M. Ward's laboratory (NIH/NINDS) by cloning human LC3A into the lentiviral vector pLEX with a PGK promotor and an EGFP tag at the N terminus of LC3. α-Synuclein-mApple was generated by Epoch Life Science Inc. by cloning human SNCA into the pLEX vector with a PGK promotor and an mApple tag at the C terminus of α-Synuclein. EGFP-LC3 was generated previously (Cheng et al., 2015). α-Synuclein-A53T-RFP was a gift from Dr. H. Cai (NIH/NIA). Stealth siRNAs are from Thermo Fisher Scientific (Arl8a/b-siRNA#1: MSS290361 and Arl8b-siRNA MSS289173; Arl8a/b-siRNA#2: Arl8a-siRNA MSS229276 and Arl8b-siRNA MSS289171). mApple-Lamp1 was from Addgene (Cat# 54627), also named mApple-Lysosomes-20. Arl8b-mCherry is a gift from Dr. J. Bonifacino (NICHD/NIH). An siRNA-resistant Arl8b mutant was created by substituting nine nucleotides in the Arl8b-siRNA#1-targeting region (G459A, T462C, A463C, A465T, A468G, T471C, C474T, C477T and T480C).

Lentivirus production and infection

HEK293T cells were transfected with vector, psPAX2, and pMD2G plasmids at a 3.6:2.8:1 ratio to produce the lentivirus. After over-night transfection, the medium was aspirated and replaced with 8 mL of DMEM medium (ThermoFisher Scientific) containing 10% Fetal Bovine Serum (HyClone). Virus-containing medium was collected after 24, 48, and 72hr, then centrifuged at 1000 g for 10 minutes to remove cell debris. The pre-cleaned virus-containing medium was aliquoted and stored at −80°C until use. For infection, 200,000 freshly dissociated neurons were incubated with 5 μl virus preparation in 20 μl plating medium for 10 min before plating in a microfluidic device.

Live neuron imaging

During live-imaging, neurons were maintained in a pre-warmed Hibernate A low fluorescence medium (BrainBits) supplemented with 2% B27 and 0.5 mM GlutaMAX. Temperature was maintained at 37°C using a stage-mounted incubator. Time-lapse images of axon bundles in the microgrooves or axonal distal ends in the axon compartment were acquired with an Olympus Fluoview FV1000 confocal microscope using a 1.45 NA 63 × objective and a CCD camera (Hamamatsu) using a mercury lamp source and a filter-wheel setup alternating GFP and Texas Red filter sets (Olympus). Alternatively, neurons were imaged with a 40 × 1.3 NA oil immersion objective on an 880 Zeiss confocal microscope. Single-color time-lapse imaging of axonal lysosomes was performed with ~1 s intervals for 3 or 5-minutes recording. Dual-color time-lapse imaging was performed with ~2 s intervals for 3 or 5-minutes recording. Kymographs were generated by ImageJ (NIH) and converted to QuickTime video.

Western blot

DRG neurons at DIV0 were nucleofected with siRNAs against Arl8a, Arl8b, or scrambled control and collected at DIV2-3. HEK293T cells were co-transfected with Arl8b-mCherry and ctrl-siRNA or Arl8a/b-siRNA#1, or R-Arl8b-mCherry + ctrl-siRNA or Arl8a/b-siRNA#1, and collected 3 days after transfection. Cells were collected and lysed with RIPA buffer (50 mM Tris-HCl, pH 7.5, 150 mM NaCl, 1% Triton X-100, 0.1% SDS, 0.5% DOC) with protease inhibitors. Equal amounts of protein lysates were then loaded and resolved on a 10% Tris-Glycine protein gel and analyzed by western blot using rabbit anti-Arl8 (1:1000, Proteintech), mouse anti-mCherry (1:2000), Abcam), anti-GAPDH (1:1000, BD Biosciences) or anti-α-tubulin (1:2000, Abcam) antibodies.

QUANTIFICATION AND STATISTICAL ANALYSIS

All quantifications were performed not blinded. Statistical parameters including the definitions and exact value of n (e.g., number of experiments or replicates, number of axons, number of organelles, number of neurons, etc), deviations and p values are reported in the figures and corresponding figure legends. Statistical analysis was carried out using Prism 7 (Graphpad Software). Statistical comparisons were performed by an unpaired t test (sample size $n \geq 30$) or Mann-Whitney test and Anova-Kruskal-Wallis test (sample size $n < 30$). Data are expressed as mean ± SEM. Differences were considered significant with $p < 0.05$.

Cell Reports, Volume *28*

Supplemental Information

Neuronal Soma-Derived Degradative Lysosomes Are Continuously Delivered to Distal Axons to Maintain Local Degradation Capacity

Tamar Farfel-Becker, Joseph C. Roney, Xiu-Tang Cheng, Sunan Li, Sean R. Cuddy, and Zu-Hang Sheng

Neuronal soma-derived degradative lysosomes are continuously delivered to distal axons to maintain local degradation capacity

Supplemental Figures

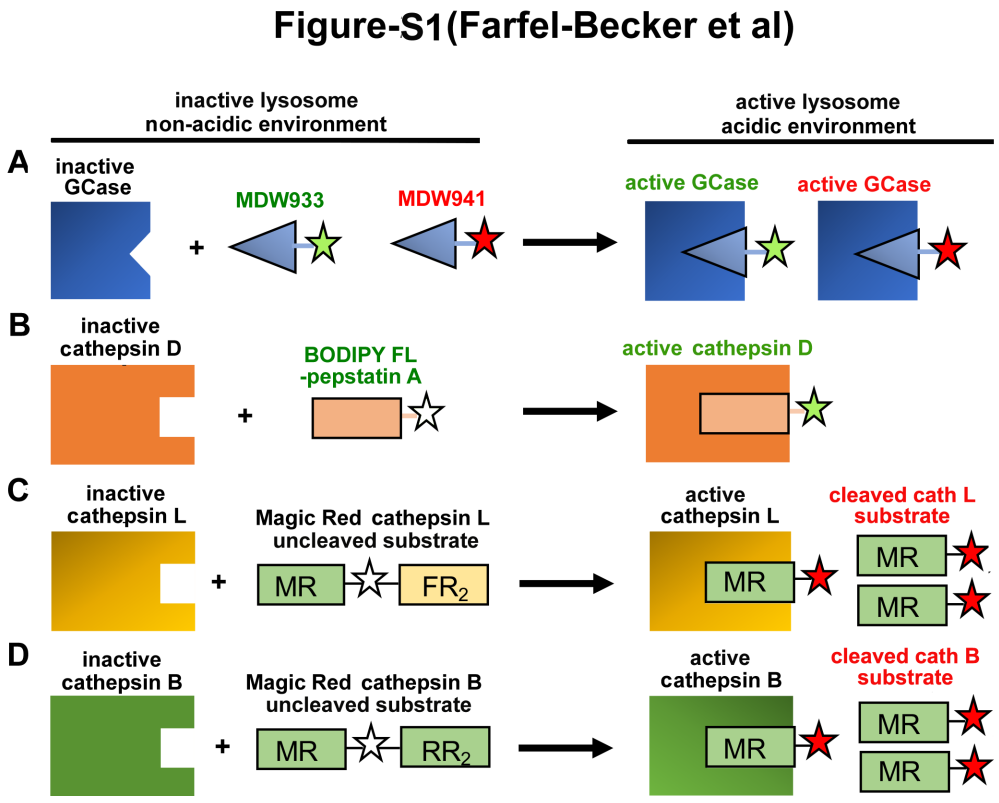

Figure S1 (related to **Figures 1** and **2**). **Illustration Showing Activity-based Fluorescent Probes for Degradative Lysosomes**

(A, B) The activity-based fluorescent probes MDW933 (green) and MDW941 (red) label active GCase (Witte et al., 2010) (A) and BODIPY-FL-pepstatin A labels active cathepsin D (Chen et al., 2000) (B). In non-acidic environment, lysosomal hydrolases are not fully active, and thus the probes will not bind their hydrolases. However, under the lysosomal acidic environment, the hydrolases become fully active, allowing the probe to bind and detect vesicular fluorescent signals indicative of enzymatically active degradative lysosomes.

(C, D) Magic Red selective fluorogenic substrates become fluorescent only upon proteolytic cleavage by cathepsin B (C) or L (D) in acidic degradative lysosomes, indicating lysosomal substrate degradation.

Figure-S2 (Farfel-Becker et al)

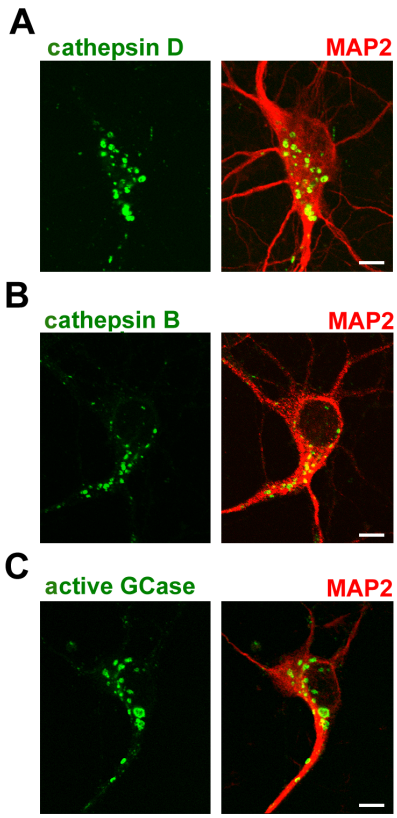

Figure S2 (related to **Figure 1B**). **Degradative Lysosomes Are Highly Enriched in the Soma**

Representative images showing the relative enrichment of degradative lysosomes within the neuronal soma. Cortical neurons at DIV7 were co-immunostained with antibodies against MAP2 and cathepsin D (A), cathepsin B (B), or loaded with MDW933 (500 nM for 1 hour) to label active GCase prior to fixation and immunostaining for MAP2 (C). Acquisition parameters were adjusted to avoid saturation of lysosomal hydrolase signals in the soma, and thus distal hydrolase signals are not readily visible. Scale bars: 5 μm.

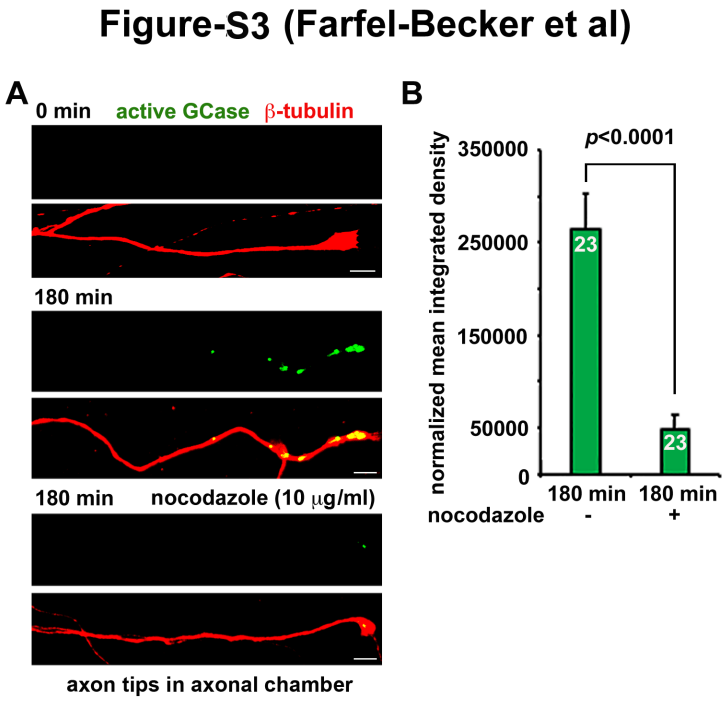

Figure S3 (related to **Figure 3**)**. Microtubule-based Axonal Transport of the Active GCase Probe MDW933 from the Soma into Distal Tips**

Representative images (A) and quantitative analysis (B) showing the microtubule-based delivery and accumulation of the active GCase probe MDW933 in distal axon tips following its loading in the soma chamber. Cortical neurons cultured in microfluidic devices were briefly labeled by the active GCase probe MDW933 (500 nM for 15 minutes) in the soma chamber at DIV7, followed by adding 10 μg/ml nocodazole to the soma chamber for 180 minutes before fixation and immunostaining for β3-tubulin. Note that the axonal delivery and tip accumulation of MDW933 signals were abolished by depolarizing microtubules in the soma chamber with nocodazole treatment. Data were quantified from 23 axon tips per condition and expressed as mean ± SEM with Anova-Kruskal-Wallis test. Scale bars: 5 μm.